

RSC Advances



This is an *Accepted Manuscript*, which has been through the Royal Society of Chemistry peer review process and has been accepted for publication.

Accepted Manuscripts are published online shortly after acceptance, before technical editing, formatting and proof reading. Using this free service, authors can make their results available to the community, in citable form, before we publish the edited article. This *Accepted Manuscript* will be replaced by the edited, formatted and paginated article as soon as this is available.

You can find more information about *Accepted Manuscripts* in the [Information for Authors](#).

Please note that technical editing may introduce minor changes to the text and/or graphics, which may alter content. The journal's standard [Terms & Conditions](#) and the [Ethical guidelines](#) still apply. In no event shall the Royal Society of Chemistry be held responsible for any errors or omissions in this *Accepted Manuscript* or any consequences arising from the use of any information it contains.

Stability of Graphene-Based Heterojunction Solar Cells

Eric Singh^{1,2} and Hari Singh Nalwa^{2*}

¹*William S. Hart High School, 24825 North Newhall Avenue, Santa Clarita, California 91321, USA*

²*Advanced Technology Research, 26650 The Old Road, Suite 208, Valencia, California 91381, USA*

*Author to whom correspondence should be addressed: Dr. H. S. Nalwa, nalwa@mindspring.com

Bulk-heterojunction (BHJ) solar cells based on organic small molecules and polymers are the focus of increasing attention by science and commerce. In organic photovoltaic devices, a conjugated polymer layer is used as the donor, while a fullerene-based derivative is used as the acceptor. Poly(3,4-ethylenedioxythiophene):poly(styrene sulfonate) (PEDOT:PSS) is one of the most common interfacial materials used for organic BHJ solar cells. However, PEDOT:PSS is acidic and hydroscopic in nature, and it inherits microstructural inhomogeneities that cause not only gradual degradation, but a complete failure of BHJ solar cell devices. There is a growing interest in graphene-based solar cells because graphene-based materials offer ease of solution processability, high optical transparency, and high power conversion efficiency. Graphene has been actively investigated for use as a transparent conducting electrode, and as a photoactive layer in fabricating solar cell devices. Power conversion efficiency in the range of 10% to 15% for graphene and inorganic semiconductor-based hybrid heterojunction solar cells, and 15.6% for graphene containing perovskite solar cells has been observed. Organic materials-based solar cells degrade not only from environmental exposure, but also from photo-oxidation caused by light illumination. In addition to higher power conversion efficiency, stability in graphene-based solar cells is critically important for commercial applications. In this review article, the stability

of graphene-based heterojunction solar cells under atmospheric conditions is evaluated. Current studies show that the insertion of a graphene buffer layer into the solar cell heterostructures stops degradation and enhances stability in solar cell devices. Long-term environmental stability of graphene-based heterojunction solar cells for commercial applications is discussed.

KEYWORDS: *Graphene, Graphene Oxide, Bulk Heterojunction (BHJ) Solar Cells, Poly(3,4-ethylenedioxythiophene):Poly(styrene sulfonate) (PEDOT:PSS), Power Conversion Efficiency, Stability of Graphene Solar Cells, Environment, Light Exposure.*

Table of Contents

1. Introduction
2. Graphene-Based Materials
3. Graphene-Based Heterojunction Solar Cells
4. Stability Problems with Organic Solar Cells
5. Stability of Graphene-Based Heterojunction Solar cells
6. Approaches for Improving Stability of Organic Solar Cells
7. Use of Graphene-Based Materials in Improving Stability of Solar Cells
8. Conclusions and Perspective

References

About the Authors

1. Introduction

For commercial applications, the long-term stability of solar cell devices against air, humidity, temperature, and light illumination over an extended period of time is of immense importance because organic solar cells degrade more rapidly under atmospheric conditions compared with their counterpart inorganic semiconductor-based solar cells such as crystalline silicon (Si), gallium arsenide (GaAs), cadmium telluride (CdTe), copper indium gallium selenide (CIGS) and multijunction solar cells. For example, silicon-based solar cells have been widely used around the world, and they exhibit excellent long-term stability; the lifetime of a crystalline silicon-based solar cell exceeds 20 years under ambient conditions [1,2]. Graphene also falls in the organic solar cell category. Organic polymers-based bulk-heterojunction (BHJ) solar cells have been extensively investigated, where an active layer of an organic conjugated polymer is used as the donor and a fullerene-based derivative is used as the acceptor. The power conversion efficiency (PCE) of organic solar cells is progressively increasing each year, polymer solar cells with highest PCEs are discussed here. Figure 1 shows the chemical structures of a few materials commonly used in fabricating organic BHJ solar cells which will be mentioned throughout this article. He et al. [3] reported a PCE of 8.24% from a conventional solar cell and 9.21% using an inverted structure ITO-cathode/PFN (poly[(9,9-bis(3-(N,N-dimethylamino)propyl)-2,7-fluorene)-alt-2,7-(9,9-octylfluorene)]/PTB7(thieno[3,4-b]thiophene/benzodithiophene:PC₇₁BM([6,6]-phenyl C₇₁ butyric acid methyl ester/MoO₃/Al/Ag anode. Liao et al. [4] fabricated a single-junction inverted polymer solar cell based on low-bandgap polymer, poly[4,8-bis(5-(2-ethylhexyl)thiophen-2-yl)benzo[1,2-b:4,5-b']dithiophene-co-3-fluorothieno[3,4-b]thiophene-2-carboxylate] (PTB7-Th) and ZnO doped Indium and fullerene derivative (InZnO-BisC₆₀) cathode interlayer. The solar cell structure ITO/InZnO-

BisC₆₀/PTB7-Th:PC₇₁BM/MoO₃/Ag showed a short-circuit current density (J_{sc}) of 17.24 mA cm⁻², an open-circuit voltage (V_{oc}) of 0.80 V, and a fill factor (FF) of 74.1%, resulting in a PCE of 10.31%. You et al. [5] reported a certified PCE of 10.6% for a polymer solar cell containing a low-bandgap polymer poly[2,7-(5,5-bis-(3,7-dimethyloctyl)-5H-dithieno[3,2-b:2',3'-d]pyran)-alt-4,7-(5,6-difluoro-2,1,3-benzothia diazole)], with a band gap of 1.38 eV. As supported by these reports, organic solar cells have broken the 10% PCE barrier. Huo et al. [6] prepared a wide-bandgap ($E_g=1.85$ eV) highly rigid backbone copolymer, poly{dithieno[2,3-d:2',3'-d']benzo[1,2-b:4,5-b']dithiophene-co-1,3-bis(thiophen-2-yl)-benzo-[1,2-c:4,5-c']dithiophene-4,8-dione} (PDBT-T1), consisting of an electron-rich DTBDT subunit and an electron-deficient 1,3-bis(5-bromothiophen-2-yl)-5,7-bis(2-ethylhexyl)-4H,8H-benzo[1,2-c:4,5-c']dithiophene-4,8-dione (T1) subunit. Single-junction PDBT-T1:PC₇₀BM:PEDOT:PSS-based organic solar cells showed a PCE of 8.3%, which increased to 9.74% when treated with 1,8-diiodooctane. Liao et al. [7] fabricated inverted polymer solar cells based on a low-bandgap polymer, poly[4,8-bis(5-(2-ethylhexyl)thiophen-2-yl)benzo[1,2-b:4,5-b']dithiophene-co-3-fluorothieno[3,4-b]thiophene-2-carboxylate] (PTB7-Th). Solar cells with ITO/ZnO and ZnO-C₆₀/PTB7-Th:PC₇₁BM/MoO₃/Ag showed PCE values of 7.64% with ZnO cathode and 9.35% with ZnO-C₆₀ cathode. Zhou et al. [8] reported a PCE of 9.0% for a single-cell ITO/PEDOT:PSS(Al)/PTB7-Th:PC₇₁BM/Al structure and a PCE of 11.3% for a tandem solar cell using different hole transport layer (HTL) materials, showing a 25% enhancement in PCE value compared with a single cell due to increased light absorption.

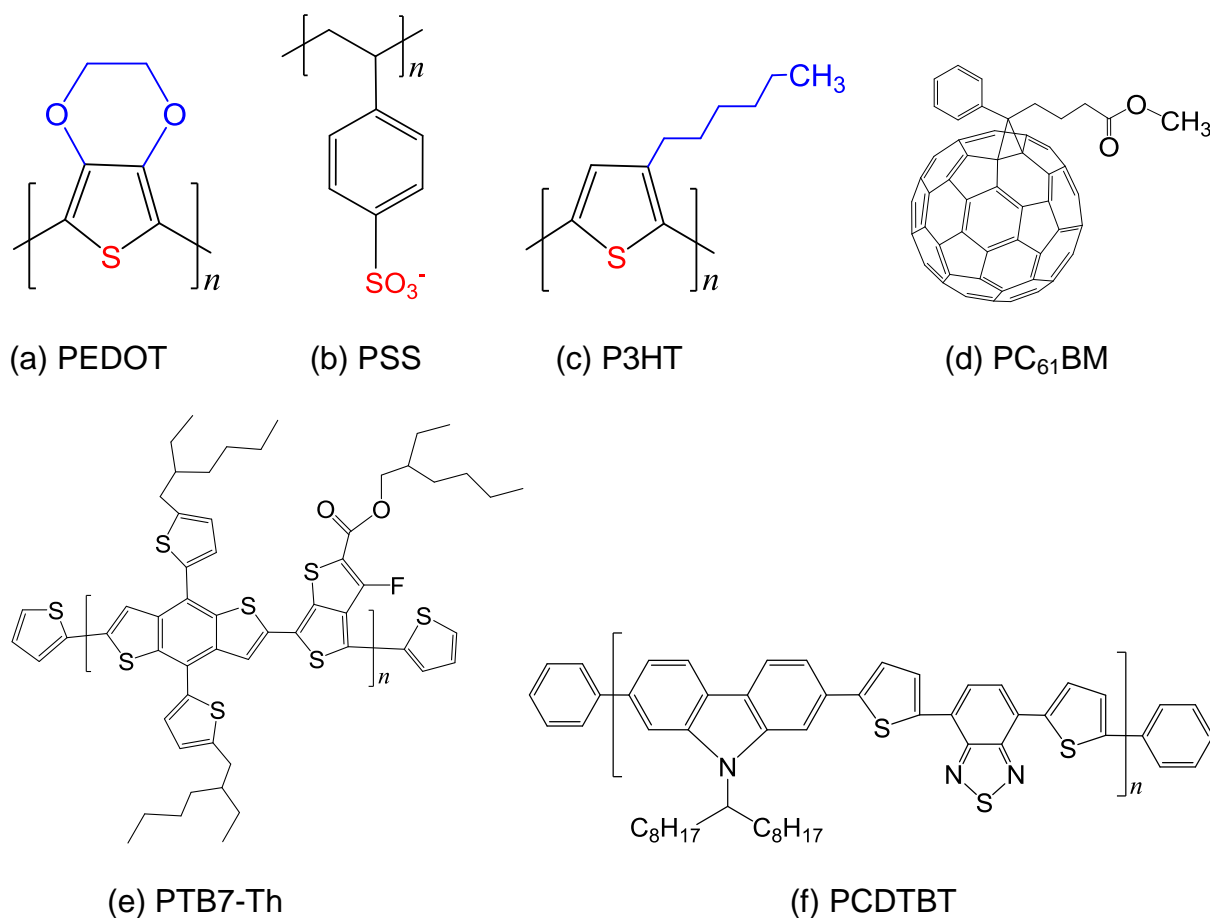


Figure 1. Chemical structures of materials in organic solar cells: (a) poly(3,4-ethylenedioxythiophene) (PEDOT); (b) poly(styrenesulfonate) (PSS); (c) poly(3-hexylthiophene) (P3HT); (d) [6,6]-phenyl-C₆₁-butyric acid methyl ester (PC₆₁BM); (e) poly[4,8-bis(5-(2-ethylhexyl)thiophen-2-yl)benzo[1,2-b:4,5-b']dithiophene-co-3-fluorothieno[3,4-b]thiophene-2-carboxylate] (PTB7-Th); and (f) poly[N-9-heptadecanyl-2,7-carbazole-alt-5,5-(4,7-di-2-thienyl-2,1,3-benzothiazole)] (PCDTBT).

Like silicon-based solar cells, the long-term environmental stability of organic BHJ solar cells is of critical importance. Physical properties such as resistance, carrier mobility, optical transparency, and power conversion efficiency for all types of organic materials in solar cell

devices change as the devices are exposed to air and other chemicals in the environment. Factors such as chemical degradation through air exposure, water absorption by hygroscopic photoactive layers, and the photo-oxidation of active layers and metal electrodes under light illumination affect and alter the overall photovoltaic performance and stability of organic materials-based solar cell devices as a function of time under different ambient conditions [9-19]. Consequently, sometimes encapsulation is employed to protect solar cell devices from air, humidity, and light exposure, and this prevents degradation.

The durability of solar cell devices is evaluated from the standpoint of chemical stability based on materials in the air, degradation caused by reactions with water and oxygen molecules, and the potential degradation of electrode materials. The lifetime of a solar cell device is governed by materials used for donor, acceptor, electrode, and buffer components. Lee et al. [20] reviewed the stability of polymer-based solar cells and pointed out that degradation arises from the macrophase separation of donor-acceptor blends, as well as the photo-oxidation of active layers and donor materials due to the diffusion of water and oxygen molecules from the interface of the interlayer/electrode. They also discussed approaches to stabilize and protect solar cell devices from degradation. To stop degradation of solar cells, improvement and stability of the morphology of donor-acceptor blends, photoactive materials, and interfaces between interlayer and metal electrode (anode, cathode) are important. Approaches such as encapsulation, photo-crosslinking, and the deposition of buffer layers in organic solar cells have been used. Potsavage et al. [21] studied the stability of ITO/pentacene/ C_{60} /bathocuproine/Al heterojunction solar cells and found that encapsulated devices with 200 nm-thick Al_2O_3 film degraded by 6% over a period of 6145 h (over 250 days) in ambient air atmosphere, compared to a ~20% drop in power conversion efficiency (PCE) after 10 h for an unencapsulated solar cell device. Kanai et

al. [22] used a molybdenum trioxide buffer layer for improving stability in organic solar cells. Jeon and Lee [23] used a phosphine oxide type cathode modification layer to improve high-temperature stability in organic solar cell devices. Wang et al. [24] enhanced stability with lithium benzoate as a cathode interfacial layer, and Søndergaard et al. [25] used polyurethane encapsulation of polymer solar cells, while Gaynor et al. [26] applied laminated nanowire electrodes to inverted polymer solar cells. Many other approaches and studies of long-term stability of organic solar cells have been reported [27-30].

2. Graphene-Based Materials

Graphene consists of a single atomic sheet of graphite, and has been extensively studied in the many research fields of science, engineering and medicine. The 2D graphene structure can be transformed into large-area stretchable ultrathin films [31-33], sheets [34-38], nanoribbons [39-41], and large-area graphene paper [42], and foams [43,44]. The graphene based materials have been used in supercapacitors [45], organic solar cells [46-49], biosensors [50], field emission cathodes [51,52] and touch screen-panel devices [53].

Graphite oxide (oxidized graphite) and graphene oxide (GO), an oxidized single- or multi-layered individual graphene sheet, are precursors to graphene (Figure 2). Various oxygen functional groups, such as hydroxyl ($-OH$), carboxyl ($-COOH$), carbonyl ($-C=O$), epoxide ($C-O-C$), and 5- and 6-membered ring lactols have been identified in graphite oxide or GO [54-56]. In connection with electrical properties and photovoltaics, few-layer graphene (FLG) exhibits very high carrier mobilities of $10,000 \text{ cm}^2/\text{Vs}$ at room temperature and 97.7% optical transparency [57]. GO, reduced graphene oxide (rGO), and graphene have been used in fabricating organic solar cells, therefore, their thermal stability is briefly discussed. GO

containing oxygen functional groups can be reduced to graphene sheet by various reduction processes, including thermal annealing at elevated temperature [58] and chemical reduction using hydrazine [59], which removes oxygen groups from GO and induces higher thermal stability and electrical conductivity. Thermal reduction of GO to graphene is associated with the elimination of carboxyl, hydroxyl, and epoxy groups, which also causes structural changes.

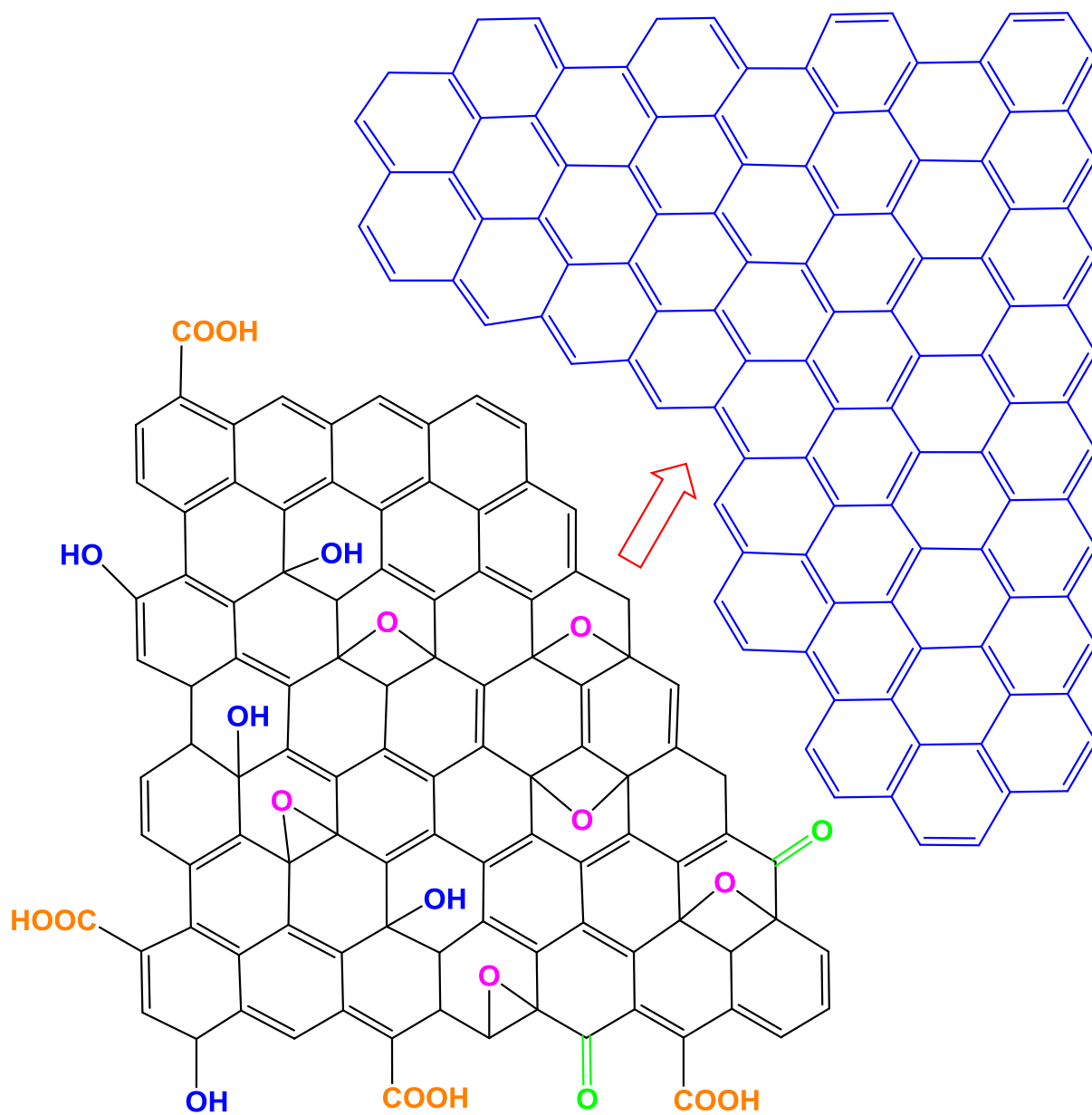


Figure 2. Chemical structures of graphene oxide (GO) and graphene. GO containing oxygen functional groups such as hydroxyl ($-OH$), carboxyl ($-COOH$), carbonyl ($-C=O$), and epoxide ($C-O-C$), can be eliminated, and GO can be reduced to graphene sheet by various reduction processes, including thermal annealing at elevated temperature and by chemical reduction, which induces higher thermal stability and electrical conductivity.

Many approaches have been employed for the reduction of GO to graphene. Wang et al. [58] reported thermal-decomposition reduction of GO to graphene in air at 300–350 °C for 1 h, with the release of O₂, CO, CO₂, and H₂O molecules from the GO surface. Mathkar et al. [59] performed a stepwise controlled study on the reduction of GO by exposure to hydrazine vapors and manipulation of its band gap by analyzing infrared absorption frequencies. Carbonyl groups were found to be reduced first; tertiary alcohol groups were the last to be removed from the GO surface. With this controlled reduction process, the optical band gap progressively changed from 3.5 eV to 1.0 eV. The XPS spectra also concurrently evidenced an increase in the C/O ratio. Park et al. [60] compared the hydrazine reduction of GO particles and exfoliated individual graphene oxide platelets. The reduced materials were found to exhibit different chemical and structural properties as analyzed by elemental analysis, TGA, XPS, XRD, and SEM methods. The hydrazine reduction of GO platelets resulted in agglomerates of exfoliated platelets, whereas the reduction of GO particles produced non-exfoliated particles. Furthermore, BET surface area and the degree of chemical reduction of rGO both were found to be lower compared to rGO. Acik et al. [61] investigated the removal of oxygen in rGO using *in situ* transmission infrared absorption spectroscopy of GO films after thermal annealing between 60 °C to 850 °C in a vacuum. They identified epoxide, hydroxyl, carboxyl, lactol, ether, and ketone groups, as well as derivatives from the spectroscopic results. The thermal reduction of GO was found to yield defective graphene structures due to remaining oxygen groups even after annealing at 850 °C. A longer annealing time was found to be more effective in removing the remaining oxygen groups, at around 600 °C.

It is important to understand the thermal stability of graphene-based materials for commercial applications. Zhang et al. [62] reported thermogravimetric analysis (TGA) of GO sheets, which showed more than 30% in 110–230 °C due to the removal of thermal-labile oxygen groups. The longer oxidation time as well as more oxidants induced much faster weight loss from 110 to 230 °C, evidencing lower thermal stability associated with more functional oxygen groups. The initial reduction of GO is accompanied by the removal of absorbed water at 100 °C and thereafter by decomposition of thermal-labile oxygen functional groups on the GO surface. Shen et al. [63] performed TGA on rGO and pointed out that the removal of oxygen functional groups significantly increased thermal stability for rGO, which exhibited 2% weight loss at 700 °C in a nitrogen atmosphere. It is evident that graphene-based materials are quite stable at moderate-to-high temperatures. The thermal-labile oxygen groups in GO give rise to low thermal stability compared with a graphene sheet, which shows stability at up to 700 °C. The structural transformation from GO to rGO and to graphene is accompanied by gradual changes in band gap, hence, electrical conductivity and thermal stability also are significantly influenced by this structural change. Both of these parameters have a significant effect on the photovoltaic properties and stability of graphene-based solar cells.

The mass production of solution-processable, chemically exfoliated GO and the dispersion behavior of GO and rGO have been reported. Sun and Gugetsu [64] reported the mass production of GO from expanded graphite using a deviation from the conventional Hummers method. Fully exfoliated GO was prepared from expanded graphite having 50-15 µm diameter as the precursors. The method facilitates the production of graphene with few functional groups, increased thermal stability, decreased resistivity, and low impurities. The traditional Hummers method inherits a low reduction rate as well as safety issues, while being safe and applicable to

the mass production of GO. In an interesting study, Konios et al. [65] reported the dispersion behavior of GO and chemically rGO in 18 different organic solvents. The variety of solvents was used to examine the effect of the reduction process on GO solubility, and was analyzed in connection with solvent polarity, surface tension, and Hansen and Hildebrand solubility parameters. The effect of the removal of oxygen-containing functional groups during the reduction process on the quality of dispersion was observed. The Hansen and Hildebrand parameters of GO and rGO indicated a strong effect of the reduction process on solubility and stability. The GO showed excellent dispersion in *N*-methyl-2-pyrrolidone (NMP), *N,N*-dimethylformamide (DMF), ethylene glycol, tetrahydrofuran (THF), and water. The solutions of GO in *N*-methyl-2-pyrrolidone (NMP), ethylene glycol, and water showed significant long-term stability. TGA was used to analyze weight loss as a function of temperature for dried GO and rGO. Absorbed water molecules from GO evaporated from room temperature to 200 °C, then the decomposition of oxygen functional groups occurred, with 40% weight loss up to 600 °C. The rGO exhibited higher thermal stability than GO due to the removal of oxygen functional groups during the reduction process.

There has been significant confusion and inconsistency with graphene-based materials, so Bianco et al. [66] attempted to classify two-dimensional (2D) graphene materials. Graphene, few-layer graphene, multi-layer graphene, graphene nanosheet, exfoliated graphite, graphene nanoribbon, graphene quantum dots, graphene oxide, graphite oxide, reduced graphene oxide, derivative terms, and other materials have been defined in detail. Wick et al. [67] suggested a classification approach for graphene-based materials (GBMs) and an excellent explanation that is summarized here. Figure 3 shows the classification grid for categorizing different graphene types according to three fundamental GBMs properties: the number of graphene layers, atomic

carbon/oxygen (C/O) ratio, and average lateral dimension. The different graphene-based materials depicted at the six corners of the box show ideal cases in accordance with lateral dimensions and the number of graphene layers reported in the literature. The values of GBMs are also shown at the nano- and micro-scale. The graphene-based materials (GBMs) consist of single-layer graphene to few-layer graphenes (i.e., 2–10 layers), graphene oxide (GO) and reduced graphene oxide (rGO) are generally a single layer, graphene nanosheets, ultrafine graphite (over 10 graphene sheets but less than 100 nm in thickness). The number of layer determines the thickness, the specific surface area, and bending elasticity. The lateral sizes of GBMs cover several orders of magnitude from the nanoscale (10 nm) to the microscale (20 mm). Pristine graphene is hydrophobic in nature whereas the GO surface consists of hydrophilic regions with hydrophobic islands. GO can be viewed as a derivative of graphene having hydroxy, carbonyl, and epoxy groups on the planar surfaces and edges.

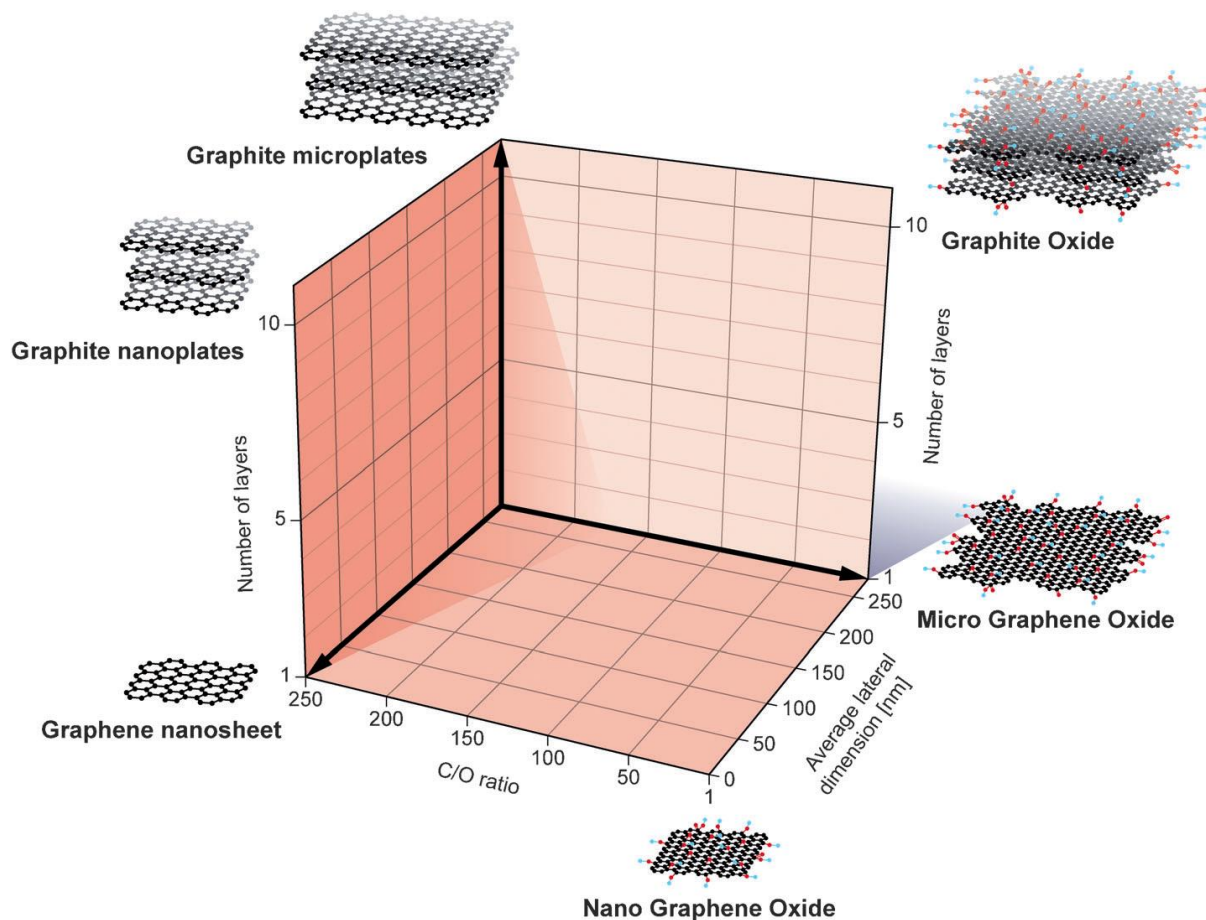


Figure 3. Classification grid for categorizing different graphene types according to three fundamental graphene-based materials (GBMs) properties: the number of graphene layers, atomic carbon/oxygen (C/O) ratio, and average lateral dimension. Reprinted with permission from Ref. 67, P. Wick, A. E. Louw-Gaume, M. Kucki, H. F. Krug, K. Kostarelos, B. Fadeel, K. A. Dawson A. Salvati, E. Vazquez, L. Ballerini, M. Tretiach, F. Benfenati, E. Flahaut, L. Gauthier, M. Prato, and A. Bianco, Classification Framework for Graphene-Based Materials, *Angew. Chem. Int. Ed.* 53, 7714-7718 (2014). Copyright © Wiley-VCH.

While Bianco et al. [66] and Wick et al. [67] classified and differentiated GBMs by explaining graphene, graphene oxide, and reduced graphene oxide, a number of reviews have been published on the nature, processability, and properties of different GBMs [68-77]. Cong et al. [78] reviewed functional GBMs with dimensionality aspects such as 1D graphene fibers/ribbons, 2D structured graphene films/papers, and 3D network-structured graphene and their composites. The most common graphene production methods, including mechanical exfoliation, liquid-phase exfoliation, ultrasonification, reduction of graphene oxide, bottom-up synthesis, epitaxial growth on SiC, and chemical vapor deposition (CVD), as well as synthetic GBMs, such as graphite oxide, graphene oxide, and reduced graphene oxide, and their processability and properties have been reviewed by Ambrosi et al. [79], Raccichini et al. [80], and Zhu et al. [81] in connection with energy storage applications.

3. Graphene-Based Heterojunction Solar Cells

Research and development on graphene-based solar cells has been rather rapid compared to organic solar cells. Currently, graphene-based solar cells show PCEs in the range of 10% to 15%, depending on the solar cell configuration and materials. A PCE of 10.56% has been observed for a 5-layer graphene/P3HT/CH₃-Si organic solar cell with a 4-mm² device area by Xie et al. [82]. In an interesting development, Tsuboi et al. [83] reported a PCE of 11.1% for a trilayer-graphene/MoS₂/*n*-Si solar cell with 9 nm-thick MoS₂ layer. Xu et al. [84] showed a PCE of 13.3% with 82.3% optical transparency for PEDOT:PSS/AgNWs/graphene oxide transparent conductive electrode (TCE)-based organic-Si hybrid solar cells. Li et al. [85] reported an experimental PCE value of 15.5% with an Al₂O₃-coated graphene/*n*-GaAs solar cell, and predicted a theoretical PCE of 25.8% for graphene/*n*-GaAs hybrid solar cells. Song et al. [86]

reported a PCE of 12.4% for graphene/*n*-silicon devices with an interfacial oxide thickness of 15 Å after chemical doping with AuCl₃, and a PCE of 15.6% after using TiO₂ antireflective coating (ARC). Yusoff et al. [87] used Au-doped single-layer graphene nanoribbons as a transparent conducting electrode instead of ITO. When Au-doped single-layer graphene nanoribbons were used in a tandem solar cell structure, a PCE of 8.48% was obtained, which is the highest efficiency for ITO-free tandem organic solar cells. The incorporation of a graphene/TiO₂ layer in a perovskite-based solar cells resulted in the highest PCE of 15.6%, as reported by Wang et al. [88]. The graphene and perovskite combination seems very interesting for enhancing the photovoltaic performance and stability of solar cell devices. Graphene-based materials have demonstrated a great potential for solar cell devices in a short span of time. Equally important is the stability of these graphene-based solar cells under ambient atmospheric conditions. In this article, current results on stability/degradation of graphene-based solar cells are discussed, and their potential for commercial applications in solar cell industries is considered. Current knowledge, as well as strategies for minimizing degradation and for improving the lifetime of graphene-based solar cells under ambient atmospheric conditions, is discussed.

4. Stability Problems with Organic Solar Cells

In general, a PEDOT:PSS blend has been widely used as an anode interfacial material in electronics and photonics because of its ease of solution processability, high electrical conductivity, and optical transparency [89, 90]. The electrical conductivity of this blend results from the doping of the conjugated polythiophene backbone-based PEDOT with polystyrene sulfonic acid. PEDOT:PSS suffers from several drawbacks that cause low stability or even a complete failure of PEDOT-PSS-based organic light-emitting diodes (OLEDs) and organic solar

cell devices. In organic solar cells, PEDOT:PSS is generally used as an interfacial material between the photoactive layer and the ITO electrode.

PEDOT:PSS has a low conductivity compared to ITO which limits its applications in devices, therefore, chemical doping and thermal annealing [91-94], as well as composites, [95] have been used to enhance the conductivity and environmental stability of solar cell devices. However, there is a tradeoff between optical transparency and electrical conductivity of a PEDOT:PSS system: higher conductivity induced by chemical doping or thermal annealing leads to decreased optical transmission, which means restricted absorption of light resulting in a lower PCE of PEDOT-PSS-based solar cell devices. To overcome this drawback and find a balance between conductivity and optical transparency, Kymakis et al. [95] used single-walled carbon nanotubes (SWCNTs)/PEDOT:PSS as the hole collecting electrode for P3HT:PCBM-based solar cells.

Spin-coated PEDOT:PSS films suffer from morphological phase segregation, which causes anisotropy in the conductivity due to the inhomogeneous distribution of conducting PEDOT and insulating PSS grains, giving rise to inhomogeneous charge extraction in solar cells. Pingree et al. [96] reported microstructural inhomogeneities in PEDOT:PSS thin films by using conductive atomic force microscopy where 20-nm size conducting regions were found to be surrounded by insulating regions. The density of the conducting PEDOT regions significantly improved by lowering the PSS amount and by increasing thermal annealing time. Nardes et al. [97] performed scanning probe microscopy with conductivity measurements to examine anisotropic conductivity of PEDOT:PSS thin films and found PEDOT-rich particles separated by quasi-continuous PSS lamellar structures. Wei et al. [98] demonstrated that the addition of ethylene glycol (EG) to PEDOT:PSS solution can significantly improve the crystallinity and

ordering of PEDOT in the solid thin films as evidenced by grazing-incidence wide angle X-ray diffraction (GIWAXD) and grazing-incidence small-angle X-ray scattering (GISAXS). It also increases the electrical conductivity of PEDOT:PSS blend due to enhanced carrier mobility and density. In context with graphene materials, Gao et al. [99] doped poly(3-hexylthiophene) (P3HT) film by depositing a thin layer of graphene oxide, which increased the electrical conductivity of P3HT by six orders of magnitude. Also, the effect of graphene oxide (GO) surface doping on inverted P3HT:PC₆₁BM solar cells was examined, where solar cell devices without a GO interfacial layer showed very poor photovoltaic performance. The inverted P3HT:PC₆₁BM solar cells with Al and Ag anodes showed PCEs of 0.21% and 0.84%, respectively, whereas with a GO interfacial layer, PCEs for GO/Al and GO/Ag anodes increased to 2.77% and 3.94%, respectively.

The deposition of a PEDOT:PSS layer is a water-borne process, therefore, thermal annealing at elevated temperature is generally used to remove water molecules from organic solar cell devices to ensure their stability under ambient conditions. The PEDOT:PSS blend being hydroscopic in character, it potentially reabsorbs moisture, which affects the performance of solar cell devices. The hydroscopic and acidic nature of the PEDOT:PSS blend plays a significant role in corroding the ITO electrode, other photoactive layers, and the processing equipment. The absorbed water vapors penetrate the active layer, degrading solar cell devices and leading to failure. Kawano et al. [100] reported photovoltaic performance of poly[2-methoxy-5-(3',7'-dimethyloctyloxy)-1,4-phenylene vinylene] (MDMO-PPV):PC₆₁BM-based solar cells fabricated on ITO glass with or without a layer of PEDOT:PSS. The studies on solar cells without any encapsulation were conducted in dark, white light irradiation, air, dry oxygen, and humid nitrogen atmospheres as a function of time. It was concluded that the degradation was

light-independent under air exposure and occurs due to the water adsorption by the hygroscopic PEDOT:PSS layer. The water-caused degradation decreases the conductivity of the PEDOT:PSS blend layer, as supported by charge mobility and hole injection measurements after air exposure. Norrman et al. [101] also showed water-induced degradation of P3HT and poly[2-methoxy-5-(2'-ethylhexyloxy)-1,4-phenylenevinylene] (MEHPPV)-based solar cell devices by using H_2^{18}O isotopic labeling experiments. Norrman et al. [17] reported degradation and failure mechanisms in inverted P3HT:PC₆₁BM solar cells with ZnO electron transporting layer and PEDOT:PSS hole transporting layer using ITO and Ag electrodes. The major failure takes place at the interface between PEDOT:PSS and the active layer because PEDOT:PSS showed phase separation, where PEDOT-rich regions degrade in an oxygen atmosphere. Both PEDOT and PSS show different reactivity toward oxygen. The device failure was found to be associated with PEDOT:PSS phase separation and at the PEDOT:PSS-active layer interface. Voroshazi et al. [102] also demonstrated the role of a PEDOT:PSS blend in the degradation of polymer:PC₆₁BM solar cells under ambient conditions in the dark. The oxidation was found to be caused by the diffusion of water vapors from the edges into the hygroscopic PEDOT:PSS layer, therefore, it was the hygroscopic nature of the PEDOT:PSS blend, not its acidity, which lead to the degradation of solar cells. When a layer of MoO₃ was used in place of the PEDOT:PSS layer, the stability of solar cell devices considerably improved.

The overall degradation of organic solar cells is a rather complicated process but to include a few important factors, it involves photo-oxidation of conjugated polymeric materials and fullerene derivatives, eroding of the ITO electrodes, loss of electrical and mechanical contacts, and morphological inhomogeneities. To overcome these drawbacks of PEDOT:PSS-

based solar cells, novel inorganic and organic materials have been studied as HTLs in BHJ solar cells.

5. Stability of Graphene-Based Heterojunction Solar Cells

Organic solar cells have been studied extensively and are of great interest to solar cell industries because of their ease of solution processability, their large-area fabrication and low weight, and because their electrical, optical, thermal, and mechanical properties can be fine-tuned [28-30, 103-106]. Graphene, because of its solution processability, high thermal and mechanical stability, as well as its high carrier mobility and excellent optical transparency, has emerged as a new candidate material for solar cells. Recently, Singh and Nalwa [107] reviewed the current status and understanding of graphene-based bulk-heterojunction (BHJ) solar cells, where graphene has been used as a transparent conducting electrode (TCE), electron transport layer (ETL), hole transport layer (HTL), or electron/hole separation layer, and as an active interfacial layer in fabricating organic and hybrid heterojunction solar cell devices. The authors discussed the role of the number of graphene layers used, chemical doping, thermal annealing, passivation, perovskite materials, and tandem solar cell structure on the photovoltaic performance of graphene-based solar cells. Singh and Nalwa [108] also reviewed current developments in graphene-based dye-sensitized solar cells (DSSCs) including graphene composites with carbon nanotubes (CNTs), titanium dioxide (TiO_2), metals, polymers, semiconductors, ionic liquids, upconversion nanoparticles, and halide perovskites. In addition, the role of processing graphene-based materials into nanoflakes, nanoparticles, multilayers, quantum dots, nanofoams, nanoplatelets, aerogels, fibers, paper, and nanosheets on photovoltaic performance was also analyzed. It is important to consider the long-term storage of graphene-based solar cell devices.

One of the causes of degradation in BHJ organic solar cells is that the interface between the hole extracting interfacial layer poly-3,4-ethylenedioxy-thiophene:poly(styrene sulfonate) (PEDOT:PSS) and the ITO anode, as pointed out by Girtan and Rusu [30], leads to failure in solar cells. Studies that reported on the long-term stability/degradation of graphene-based solar cell devices (mainly on graphene/*n*-silicon heterojunction devices, but with a few other BHJ configurations) in terms of PCE (η) as a function of time in the air atmosphere are summarized in Table 1 [116-132]. Some of the reported data on chemical degradation and photo-oxidation are analyzed in detail here.

A poly(3,4-ethylenedioxythiophene):poly(styrene sulfonate) (PEDOT:PSS) blend has been used as a HTL in organic solar cells. However, it is highly acidic in nature so it inherits high chemical reactivity with water molecules that are present in air, and which corrode the ITO electrode and degrade the performance of polymer solar cells [9-20]. Liu et al. [109] used thermally reduced graphene oxide (GO) as an HTL in fabricating BHJ solar cell devices. It was found that the annealing temperature influences the conjugated structure of the graphene sheet and therefore the electrical conductivity of GO. Solar cell devices containing 230 °C reduced GO as the HTL exhibited a larger fill factor (FF) than solar cell devices containing 130 °C reduced GO as the HTL. The higher electrical conductivity of GO annealed at elevated temperature results from the removal of oxygen functional groups from the graphene sheet. The work function of GO can be lowered by increasing the reduction temperature, which leads to decreased open-circuit voltage (V_{oc}) for high-temperature reduced GO solar cell devices. The 26% higher PCE of GO-based devices compared to bare ITO based solar cell devices without any HTL was achieved by optimizing the concentration and spin-coating speed of GO

dispersion. The PCE of the GO-based solar cell device was 85% compared to the PCE of the PEDOT:PSS-based device.

The electron-blocking PEDOT:PSS layer also affects the photovoltaic performance of organic solar cells. Murray et al. [110] reported that the PCE and durability of organic solar cells suffer from an electron-blocking PEDOT:PSS layer. Replacing the PEDOT:PSS layer with GO significantly improved durability in solar cell devices. PCEs of 7.46% for PEDOT:PSS and 7.39% for GO interfacial layers were recorded. Figure 4 shows the stability characteristics of PTB7:PC₇₁BM solar cells with traditional PEDOT:PSS and GO interfacial layers in terms of the variation of normalized efficiency for thermal and environmental degradation of solar cell devices, with and without encapsulation. PEDOT:PSS-based solar cell devices degrade more rapidly, while GO-based devices show an initial degradation in efficiency and thereafter slower degradation, resulting in 5-fold improvement in PCE retention. A lifetime of 1428 h for PEDOT:PSS and 7156 h for GO-based solar cell devices were extrapolated. At 80% relative humidity, solar cells fabricated with GO showed retention of PCE for longer times compared with PEDOT:PSS-based devices. A lifetime of 6 h for PEDOT:PSS and 122 h for GO-based solar cell devices were extracted from degradation data. Because it is hygroscopic, the PEDOT:PSS layer attracts water molecules that cause instability and lead to degradation of unencapsulated solar cells under ambient conditions with 80% relative humidity. Solar cells based on GO showed a PCE of 7.5%, as well as 5-fold and 20-fold improvement over the lifetime for thermal aging and 80% humid conditions, respectively, compared to PEDOT:PSS-based solar cell devices. This study shows that the use of a thermally stable and mechanically strong GO layer in place of a PEDOT:PSS layer induces significantly improved stability in organic solar cells. Improved stability in organic solar cells also was observed by Kwon et al.

[111], who reported a longer lifetime of UV/ozone-treated graphene sheets as hole extraction layer (HEL) compared to PEDOT:PSS-based solar cells. The sheet resistance was found to increase from 1.1 k Ω /sq to infinity while the optical transmittance decreased from 95.2% to 93.8% at 550 nm, and work function increased from 4.3 eV to 4.85 eV after 9 min UV-ozone treatment because of carbon–oxygen functionalization layers. The solar cell with 5 min UV-ozone treated graphene HEL showed the highest PCE of 3.0% because the graphene sheet damaged after 7 min UV-ozone exposure. The PCE of the PEDOT:PSS-based solar cell device dropped to 0% after 14 h under humid conditions while the UV/ozone-treated graphene-based solar cell device continued to operate for 26 h. This shows that UV/ozone-treated graphene provides stability as a HEL layer in solar cells compared to a PEDOT:PSS layer.

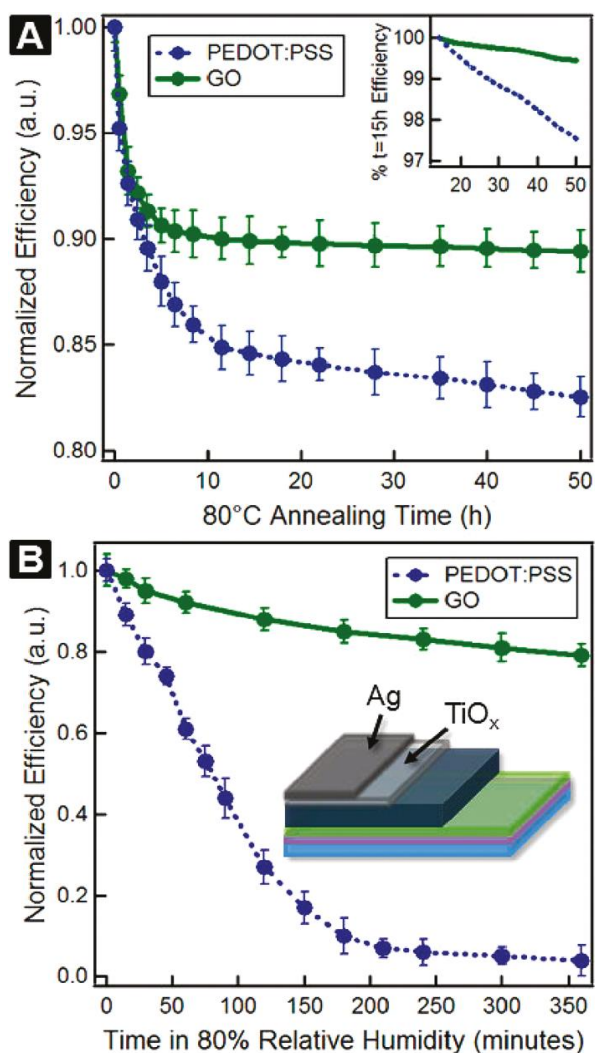


Figure 4. Stability characteristics of PTB7:PC₇₁BM-based solar cells with traditional PEDOT:PSS and GO interfacial layers. Here, poly[[4,8-bis[(2-ethylhexyl)oxy]benzo[1,2-b:4,5-b⁰]dithiophene-2,6-diyl][3-fluoro-2-[(2-ethylhexyl)carbonyl]-thieno[3,4-b]thiophenediyl]] (PTB7) is an electron donating polymer, while [6,6]-phenyl-C₇₁-butyric-acid-methyl-ester (PC₇₁BM) is the fullerene-based electron acceptor. (A) Variation of normalized PCE showing thermal degradation of encapsulated solar cell devices at 80 °C under nitrogen atmosphere. Inset: Plot of the data between 15 h and 50 h. (B) Variation of normalized PCE showing environmental degradation of unencapsulated solar cell devices. Inset: Schematic of the solar cell device used

for humidity testing. Reprinted with permission from Ref. 110. I. P. Murray, S. J. Lou, L. J. Cote, S. Loser, C. J. Kadleck, T. Xu, J. M. Szarko, B. S. Rolczynski, J. E. Johns, J. Huang, L. Yu, L. X. Chen, T. J. Marks, and M. C. Hersam, Graphene oxide interlayers for robust, high-efficiency organic photovoltaics, *J. Phys. Chem. Lett.* 2, 3006-3012 (2011). Copyright © 2011 American Chemical Society.

For the fabrication of organic solar cells, Kim et al. [112] used solution-processed GO as an anode buffer layer and compared photovoltaic performance with indium zinc oxide (IZO), IZO/GO, GO/IZO, and PEDOT:PSS-based devices, which showed PCEs of 3.4%, 3.5%, 3.9%, and 3.4%, respectively. Solar cell devices with GO as an anode buffer layer showed no degradation after light illumination for 1 h, therefore, a GO/IZO anode buffer layer provided stability, whereas devices with no GO layer exhibited very significant degradation under similar conditions. The PCE of GO/IZO-based devices decreased by 2.81% after continuous illumination for 5 h. This study shows that the GO buffer layer improved the stability of solar cells compared with conventional devices. In another study, Yang et al. [113] used a spin-coated 2 nm-thick GO buffer layer on an ITO electrode without any other treatment. The solar cell device had a configuration of ITO/GO(0–8 nm)/CuPc (35 nm)/C₆₀(40 nm)/BPhen (10 nm)/Al. The 2 nm-thick, 4 nm-thick, and 6 nm-thick GO buffer layer-based solar cells showed PCEs of 1.9%, 1.7%, and 1.0%, respectively. With the addition of a GO buffer layer, the PCE of the CuPc/C₆₀-based solar cell device increased from 1.5% to 1.9% showing, a 30% enhancement. Both CuPc/C₆₀ devices had similar structural configurations and encapsulation, except for a 2 nm-thick graphene oxide buffer layer. The standard CuPc/C₆₀-based solar cell showed a 0.001

drop in initial PCE value after 60 days, while solar cells with a GO buffer layer retained 84% of initial PCE value after 132 days. Therefore, the stability of the solar cells was significantly enhanced by the addition of a GO buffer layer. Figure 5 shows the variation of PCE response of an encapsulated ITO-based device and a GO-buffered device as a function of time stored in a glovebox after fabrication. The 2 nm-thick GO-buffered device showed an improvement in the stability of the CuPc/C₆₀ device by the addition of a spin-coated GO buffer layer on the ITO substrate. The current density–voltage characteristics of an encapsulated ITO-based CuPc/C₆₀ device at 0, 12, 24, 36, 48, 54, and 60 days, and the current density–voltage characteristics of a GO buffer layer–based CuPc/C₆₀ device at 0, 12, 24, 36, 60, 96, and 132 days of storage time is shown in Figure 6. The *J-V* curves show continuous decay in the non-buffered ITO-based solar cell device, while the *J-V* curves of the GO-buffered solar cell devices show only slight changes after 30 days of storage. The GO-buffered solar cell device retained 78% of its original PCE value after 205 days of storage. The improvement in stability results from the GO layer diffusion barrier, which stops the diffusion of oxygen molecules from ITO electrode to the active layers.

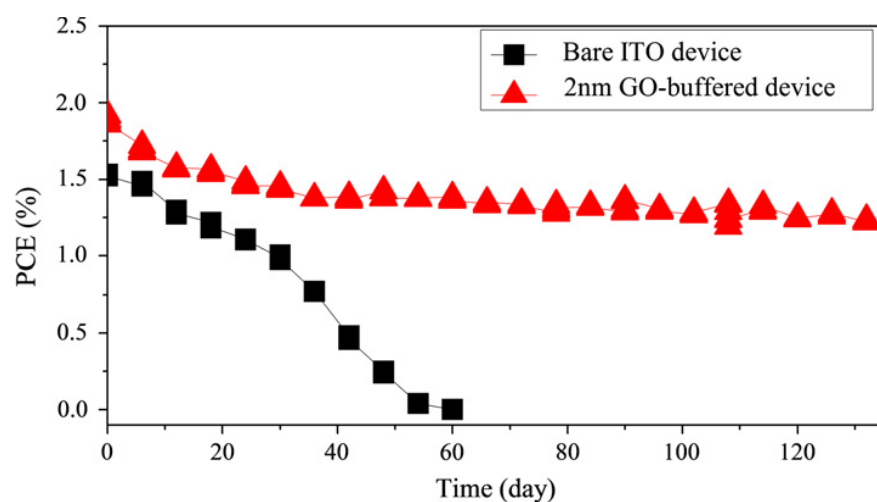


Figure 5. Variation of PCE response of an encapsulated ITO-based device and GO-buffered device. The solar cell device has a configuration of ITO/GO(0–8 nm)/CuPc (35 nm)/C₆₀(40 nm)/BPhen (10 nm)/Al. Improvement is observed in the stability of the CuPc/C₆₀ device by the addition of a spin-coated GO buffer layer on the ITO substrate without any further treatment. Reprinted with permission from Ref. 113, Q.-D. Yang, T.-W. Ng, M.-F. Lo, N.-B. Wong, and C.-S. Lee, Enhanced storage/operation stability of small molecule organic photovoltaics using graphene oxide interfacial layer, *Organic Electronics* 13, 3220-3225 (2012). Copyright © 2012 Elsevier.

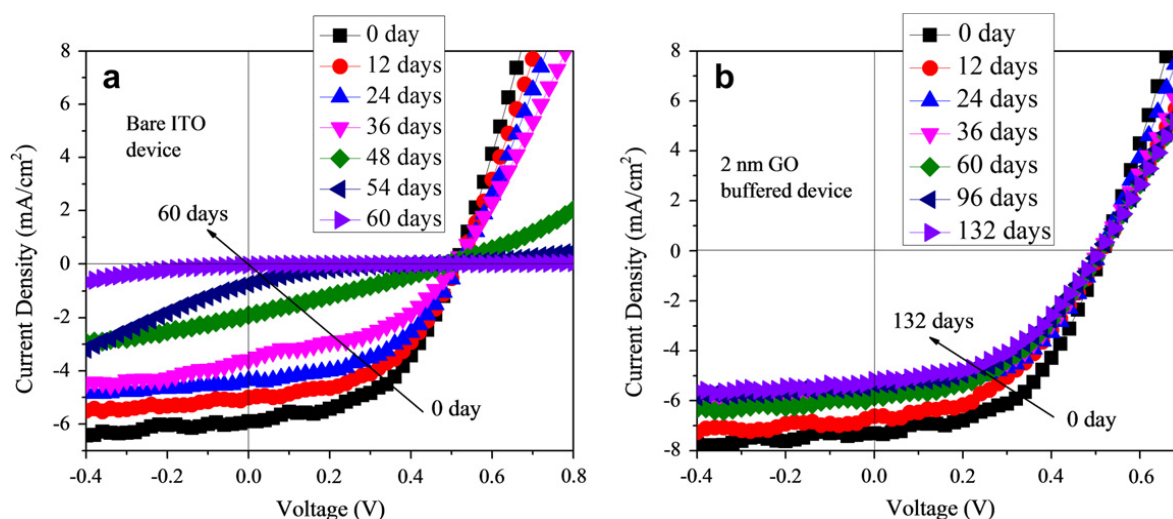


Figure 6. Current density–voltage (J - V) characteristics of encapsulated (a) ITO-based CuPc/C₆₀ device at 0, 12, 24, 36, 48, 54, and 60 days of storage time; and (b) GO buffer layer–based CuPc/C₆₀ device at 0, 12, 24, 36, 60, 96, and 132 days of storage time. Reprinted with permission from Ref. 113, Q.-D. Yang, T.-W. Ng, M.-F. Lo, N.-B. Wong, and C.-S. Lee, Enhanced storage/operation stability of small molecule organic photovoltaics using graphene oxide interfacial layer, *Organic Electronics* 13, 3220-3225 (2012). Copyright © 2012 Elsevier.

Silver nanowires (AgNWs) and graphene hybrids also have been used for solar cells. Lee et al. [114] prepared organic P3HT:PCBM solar cell devices with a AgNWs-graphene hybrid transparent conducting electrode, where CVD-grown monolayer graphene was deposited onto pristine AgNWs. The AgNWs-graphene hybrid-based TCE showed enhanced stability against thermal oxidation and chemicals because the graphene layer provided a better gas barrier. Solar cell devices fabricated with a AgNWs-graphene hybrid also exhibited high photovoltaic performance and long-term stability under ambient atmospheric conditions. In another study, Ahn et al. [115] used solution-processable anode layers of AgNWs-rGO hybrid TCE for fabricating BHJ solar cells with a PEDOT:PSS/P3HT:PCBM blend and LiF/Al cathode. The TCE based on a AgNWs-rGO hybrid showed better optical transparency and a lower sheet resistance (R_{sh}) than that of an ITO electrode, as well as increased stability against thermal oxidation and chemicals. The AgNWs-rGO electrode-based solar cells exhibited a short-circuit current density (J_{sc}) of 6.38 mA/cm², an open-circuit voltage (V_{oc}) of 0.49 V, and a fill factor (FF) of 32.91%, yielding a PCE of 1.03%. In comparison, a AgNWs transparent electrode-based control device showed a J_{sc} of 6.42 mA/cm², a V_{oc} of 0.49 V, and a FF of 38.25%, resulting in a PCE of 1.20%. To examine the effect of a rGO layer on the thermal oxidation stability of solar cells, both AgNWs and AgNWs-rGO films were exposed to 70 °C and 70% relative humidity for 8 days. Although no change in optical transmittance was observed for either, the R_{sh} of AgNWs film was found to increase >300%. In comparison, the R_{sh} of the AgNWs-rGO film showed a <50% increase under similar conditions. Such a big change in R_{sh} confirms that AgNWs-rGO films are more thermally stable against oxidation than AgNWs film because of the

impermeability of a GO layer to oxygen molecules. The R_{sh} slightly decreased for AgNWs-rGO film after 48 h because of the enhanced electrical conductivity of rGO. The study shows that AgNW-rGO film provides high thermal oxidation stability than that of AgNW film due to added rGO layer which is impermeable to oxygen molecules. Yang et al. [116] studied the stability of monolayer graphene-AgNWs-silicon solar cells at 25 °C and 60% humidity. The PCE of these graphene-AgNWs-Si cells was found to decrease by 3%, from 8.68% to 8.42%, over a period of 7 days.

It is known that PEDOT:PSS blends have some disadvantages, being acidic and hydroscopic in nature, which adversely affects the performance of organic BHJ solar cells. Yeo et al. [117] reported that a PEDOT:PSS-based solar cell completely deteriorated and failed: its PCE was 0% just after 5 days of exposure to ambient conditions due to the erosion of ITO electrodes. The hygroscopic and acidic nature of the PEDOT:PSS layer also facilitated the decomposition of perovskite components in solar cell devices. However, rGO-based solar cell devices retained 62% of initial value of PCE (9.95%) up to nearly 6 days, showing better environmental stability, as opposed to the complete failure of the PEDOT:PSS solar cell devices. Yun et al. [118] used traditionally reduced GO and *p*-toluenesulfonyl hydrazide (*p*-TosNHNH₂)-reduced GO (pr-GO) thin films as an anode interfacial layer in solar cells in place of a PEDOT:PSS layer to induce high PCE and stability in solar cells. The pr-GO-based solar cells showed an average PCE of 3.63%, which was comparable to PEDOT:PSS-based solar cells. The PCE of a PEDOT:PSS-based solar cell dropped to 0% after exposing the device to air for 8,640 min (144 h, or 6 days), whereas the pr-GO-based solar cell retained 64% PCE of its initial value after air exposure for 8,640 minutes. Furthermore, after air exposure for 18,720 minutes, the PCE of pr-GO-based solar cells still retained 54% of their initial PCE. This clearly shows pr-GO-

based solar cells have better stability against oxygen and moisture than conventional PEDOT:PSS blend-based solar cell devices.

Different aspects of the stability/degradation of graphene-based BHJ solar cells have been studied. Liu et al. [119] reported that multilayer-graphene solar cell devices showed better stability than monolayer-graphene and control devices, because multiple layers of graphene provide more resistance against air. Cui et al. [120] reported the effect of doping and stability of SOCl_2 , H_2O_2 , HNO_3 , and HCl doped graphene-based solar cells. The PCE values increased to 230% for SOCl_2 , 213.1% for HNO_3 , 212.2% for H_2O_2 , and 211.6% for HCl of their original PCEs. A pristine graphene/*n*-Si solar cell showed PCE of 2.58% which increased to 5.95% after SOCl_2 doping. The pristine graphene film showed a sheet resistance (R_s) of 1053 $\text{k}\Omega/\text{sq}$, which decreased to 650, 598, 581, and 514, Ω/sq for H_2O_2 , HCl , HNO_3 and SOCl_2 after doping treatment, respectively, indicating that the electrical conductivity of graphene increased after doping. A loss of 45% in PCE over a period of 8 days in the air for nitric acid (HNO_3)-doped graphene/*n*-silicon solar cells was observed. The PCEs retained an enhancement of 21.7% for SOCl_2 , 17.6% for HCl , 13.6% for HNO_3 and 7.4% for H_2O_2 doped solar cells compared with pristine graphene/*n*-Si solar cell, after storing for 8 days in the air. In another study, Xie et al. [121] studied graphene/silicon hole array solar (SiHA) cells where micro-hole SiHA were fabricated by photolithography. Figure 7 shows the photovoltaic characteristics of graphene/Si SiHA Schottky junction solar cell devices as a function of time. The micro-hole SiHA with 12.8- μm hole depth, along with AuCl_3 -doped graphene, showed a PCE of 10.40% for the graphene/SiHA solar cell devices. The PCE of graphene/Si SiHA Schottky junction solar cell devices was found to be hole depth-dependent, where PCEs of 6.30%, 7.89%, 9.21%, and 10.40% were measured for 3.8-mm, 6.4-mm, 10.2-mm, and 12.8-mm hole depths, respectively.

The J_{SC} values also increased significantly from 20.19 mA cm^{-2} for $3.8 \text{ }\mu\text{m}$ -thick SiHA to 31.56 mA cm^{-2} for $12.8 \text{ }\mu\text{m}$ -thick SiHA-based solar cells due to the high light absorption by thick micro-hole SiHAs. The stability of graphene/SiHA solar cells was substantially improved. The initial PCE of 10.40% for AuCl_3 -doped graphene/SiHA solar cells dropped to 9.65% after 1 week, showing a 7.2% decrease. Furthermore, the PCE value dropped to 8.38% after 1 month and to 7.42% after 3 months storage in air. After 3 months, solar cells retained 71% of the original PCE value due to the degradation of the AuCl_3 dopant over time. AuCl_3 -doped graphene/SiHA solar cells were more stable than conventional, volatile oxidant-doped solar cells. As evident here, chemically doped graphene-based solar cells suffer significantly more degradation than undoped devices because of the chemical doping effect.

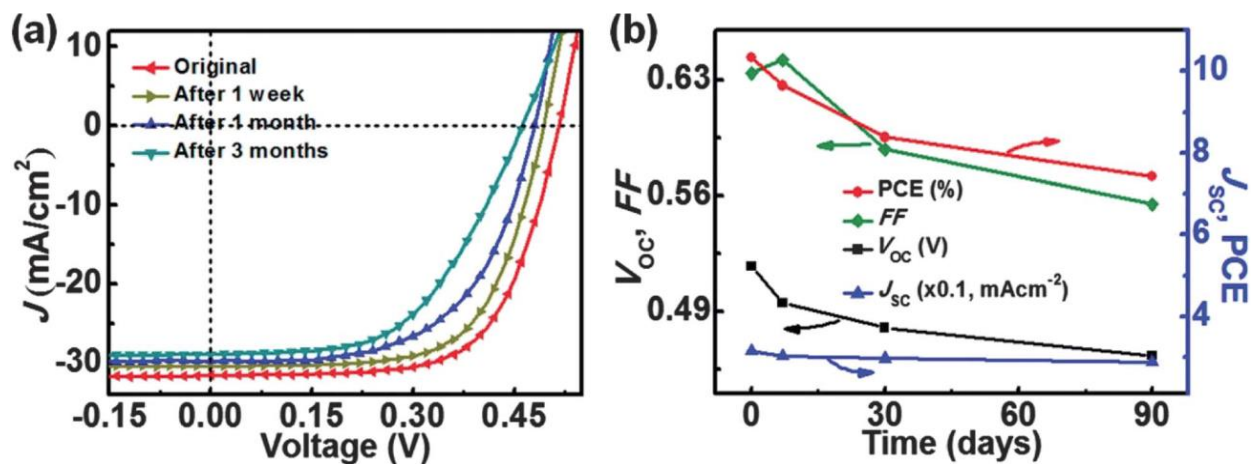


Figure 7. (a) Photovoltaic characteristics of a graphene/Si hole array (SiHA) Schottky junction solar cell device over time. (b) Plots of photovoltaic parameters as a function of time. Reprinted with permission from Ref. 121, C. Xie, X. Zhang, K. Ruan, Z. Shao, S. S. Dhaliwal, L. Wang, Q. Zhang, X. Zhang, and J. Jie, High-efficiency, air stable graphene/Si micro-hole array Schottky

junction solar cells, *J. Mater. Chem. A*, 1, 15348-15354 (2013). Copyright © Royal Society of Chemistry.

In a similar type of study, Zhang et al. [122] developed graphene/Si nanoarray Schottky junction solar cells using a Si nanowire (SiNW) array and a Si nanohole (SiNH) array. Surface charge recombination, graphene conductivity, and work function were found to determine the performance of solar cell devices. The suppression of the surface recombination with surface passivation, the number of graphene layers, and doping levels significantly enhanced the PCE of solar cells. When a P3HT thin layer was inserted as the electron blocking layer between graphene film and Si nanoarrays, maximum PCE values of 8.71% and 10.30% were obtained for SiNW and SiNH arrays-based solar cells, respectively. The HNO₃-doped graphene/SiNW array and graphene/SiNH array-based solar cells showed PCE values of 6.85% and 7.65%, respectively. The PCEs of graphene/SiNW array and graphene/SiNH array-based devices dropped 34.9% and 66.4% after 1 week, respectively.

Table 1. Long-term stability and degradation of graphene-based heterojunction solar cell devices in terms of PCE (η) as a function of exposure time under ambient atmospheric conditions.

Solar Cell Device	Power Conversion Efficiency (η)		Exposure Time	Ref.
	Initial PCE Value	PCE after Degradation		
	Graphene/ <i>n</i> -Si (HNO ₃ -doped)	5.47	2.96	8 days
Graphene/ <i>n</i> -Si (SOCl ₂ -doped)	5.95	3.29	8 days	[120]

Graphene/ <i>n</i> -Si (H ₂ O ₂ -doped)	5.12	2.37	8 days	[120]
Graphene/ <i>n</i> -Si (HCl-doped)	4.93	3.19	8 days	[120]
pr-GO ^a	3.63	2.0	13 days	[118]
Monolayer graphene/AgNWs-Si	8.68	8.42	7 days	[116]
4-layer graphene/SiHA (AuCl ₃ -doped)	10.40	9.65	7 days	[121]
4-layer graphene/SiHA (AuCl ₃ -doped)	10.40	8.38	1 month	[121]
4-layer graphene/SiHA (AuCl ₃ -doped)	10.40	7.42	3 months	[121]
Graphene/SiHA (HNO ₃ -doped)	7.65	2.57	7 days	[122]
Graphene/SiNWA (HNO ₃ -doped)	6.85	4.46	7 days	[122]
TiO ₂ /monolayer graphene/Si	14.1	6.50	20 days	[123]
Monolayer graphene/ <i>n</i> -Si-CH ₃ (passivated)	4.20 ^b	3.70	28 days	[124]
	2.0 ^c	1.5	28 days	[124]
CVD-Graphene/ <i>n</i> -Si (HNO ₃ -doped)	5.0	4.20	15 days	[125]
CVD-Three-layer Graphene// <i>n</i> -Si	5.48	4.84	1 month	[137]
PEDOT:PSS/PCDTBT:PC ₇₁ BM/GO	6.72	6.52	30 days	[129]
PEDOT:PSS/PCDTBT:PC ₇₁ BM/GO/TiO ₂	7.17	6.85	30 days	[129]
PEDOT:PSS/PCDTBT:PC ₇₁ BM/GO/TiO ₂ (in N ₂)	7.50	7.24	30 days	[129]
PEDOT:PSS/PCDTBT:PC ₇₁ BM/TiO ₂	7.02	6.80	30 days	[129]
PEDOT:PSS/PCDTBT:PC ₇₁ BM reference	5.23	2.32	30 days	[129]
ITO/rGO ^d /CH ₃ NH ₃ PbI ₃ /PC ₆₁ BM/BCP/Ag	9.95	6.0	140 hours	[117]
ITO/ZnO:Cs ₂ CO ₃ /P3HT:PCBM/GO:PEDOT:PSS/Al	3.33	2.62	28 days	[132]

ITO/ZnO:Cs ₂ CO ₃ /P3HT:ICBA/GO:PEDOT:PSS/Al	3.70	3.38	28 days	[132]
--	------	------	---------	-------

^aReduced GO (pr-GO) by *p*-toluenesulfonyl hydrazide (*p*-TosNHNH₂)

^bPCE recorded at 20 mW/cm² at AM 1.5 light source

^cPCE recorded at 100 mW/cm² at AM 1.5 light source

^drGO = reduced GO

The graphene and carbon-nanotubes based solar cells were comparatively investigated. Shi et al. [123] reported lower PCEs for graphene/Si cells than for corresponding CNT-Si solar cells. Graphene/Si solar cells showed a PCE of 3.78%, which was enhanced to 8.91% after HNO₃ doping, and then further improved to 14.1% with TiO₂/HNO₃ treatment. A colloidal antireflection TiO₂ coating was applied on a monolayer graphene/Si solar cell, which enhanced PCE to 14.5%. When a TiO₂-graphene-Si solar cell was stored in air for 20 days to test for stability, V_{OC} decreased from 0.60 V to 0.45 V, FF dropped from 73% to 45%, J_{SC} remained unchanged, and PCE decreased by 54%. The PCE of the solar cell recovered to 14.5% after doping with HNO₃ vapor, which demonstrates that it is a reversible process. On solar cell devices, chemical dopants gradually begin to evaporate or degrade after air exposure at elevated temperature and humidity over a period of time; this consequently decreases both the electrical conductivity and PCE due to degradation. As with doping, the PCE of the solar cell also recovered after applying TiO₂ antireflection coating, which seems to be a practical strategy for impeding degradation. Brus et al. [124] studied the stability of undoped graphene-Si solar cells, where the Si surface was passivated with H and CH₃ groups. The H-terminated graphene-Si solar cell device showed a very low PCE of 0.1%, whereas PCEs of CH₃-terminated devices were 2%

at 100 mW and 4.2% at 20 mW, which dropped to 1.5% and 3.7%, respectively, after 28 days in ambient conditions. It is clearly seen here that CH₃-passivated Si surfaces induced both higher PCEs and stability in graphene/*n*-Si heterojunction solar cells. Lancellotti et al. [125] reported a PCE of 5% for graphene/*n*-Si solar cells that were annealed at 200 °C, and thereafter were immediately exposed to HNO₃ vapors; the PCE retained 80% of its original value after 15 days in air. A PCE of 3.4% was recorded for a graphene/*n*-Si device with no annealing before doping, which dropped to 1.8% after 15 days in air storage. Li et al. [126] reported the effect of thionyl chloride (SOCl₂) doping on graphene/*n*-silicon Schottky junction solar cells. The chemical doping increased electrical conductivity of graphene film, which resulted in a 3-fold increase in PCE. The pristine graphene/*n*-Si solar cell showed a *J*_{sc} of 12.7 mA/cm², a *V*_{oc} of 0.42V, and a fill factor (FF) of 35%, corresponding to a PCE of 1.84%. After SOCl₂ doping, all photovoltaic parameters increased: *J*_{sc} to 13.2 mA/cm², *V*_{oc} to 0.52V, and FF to 58%, and PCE increased to 3.93%. The stability of the SOCl₂-doped graphene/*n*-Si solar cell was examined for a period of 9 days. Photovoltaic parameters decreased, confirming degradation of the solar cell performance. Where the PCE was found to stabilize at 2.5% after one week, PCE still remain higher than the original PCE value of 1.84% for the solar cell before chemical doping. The decrease in PCE value may be attributed to the volatility of the SOCl₂ dopant.

For fabricating BHJ solar cells, Yang et al. [127] used cesium carbonate (Cs₂CO₃)-functionalized graphene quantum dots (GQDs) as an electron-selective layer to fabricate BHJ solar cells. The photovoltaic properties of solar cell devices with ITO/Cs₂CO₃ or GQDs-Cs₂CO₃/P3HT:PCBM/V₂O₅/Au with different ratios of GQDs to Cs₂CO₃ were fabricated. Figure 8 shows a schematic inverted P3HT:PCBM solar cell structure with a GQDs-Cs₂CO₃ buffer layer and energy band diagram, where the energy level of the buffer layers was calculated

using UV-Vis and UPS measurements, as well as the changes in PCE, V_{OC} , FF, and J_{SC} as a function of storage time of P3HT:PCBM inverted solar cell devices containing Cs_2CO_3 and GQDs- Cs_2CO_3 buffer layer in air at room temperature and 65% relative humidity without encapsulation. The better hole-blocking ability of a GQDs- Cs_2CO_3 layer is supported by the fact that the buffer layer-modified ITO showed the valence band maximum at 3.16 eV below the Fermi level. The maximum PCE of GQDs- Cs_2CO_3 solar cells annealed at 120 °C was 3.23% compared to a PCE of 2.72% for Cs_2CO_3 -based devices under similar experimental conditions. Interestingly, the V_{oc} of a GQDs- Cs_2CO_3 device remained at 99.4% of its initial value after 1200 h of exposure in air, whereas the V_{oc} of solar cell devices with a Cs_2CO_3 buffer layer decreased rapidly with time. Both solar cell devices showed a similar degradation trend of J_{sc} . The GQDs- Cs_2CO_3 -based solar cells showed a 56% higher PCE and 200% improvement in stability compared to Cs_2CO_3 -buffered solar cell devices. The PCE of GQDs- Cs_2CO_3 -based solar cells remained at 70% of its original PCE value after 450 h of exposure to air at room temperature and 60% relative humidity; the stability was two times better compared to Cs_2CO_3 -based devices. GQDs- Cs_2CO_3 solar devices show better hole-blocking and electron transfer capability, and they inhibit diffusion of the Cs^+ ion into the buffer/polymer interface. This helps provide increased stability in solar cell devices. Liu et al. [128] compared the stability of a GO nanoribbon (GOR)-based solar cell device to a PEDOT:PSS device after unencapsulation and storage in a nitrogen gas (N_2)-filled glovebox. The PCE of the ITO/PEDOT:PSS-based device dropped to 75% after 90 days, whereas the GOR/P3HT:PCBM (200 nm)/Al (100 nm) device retained 86% of its original PCE value under similar conditions, showing that GOR as a hole extraction interfacial layer introduces stability.

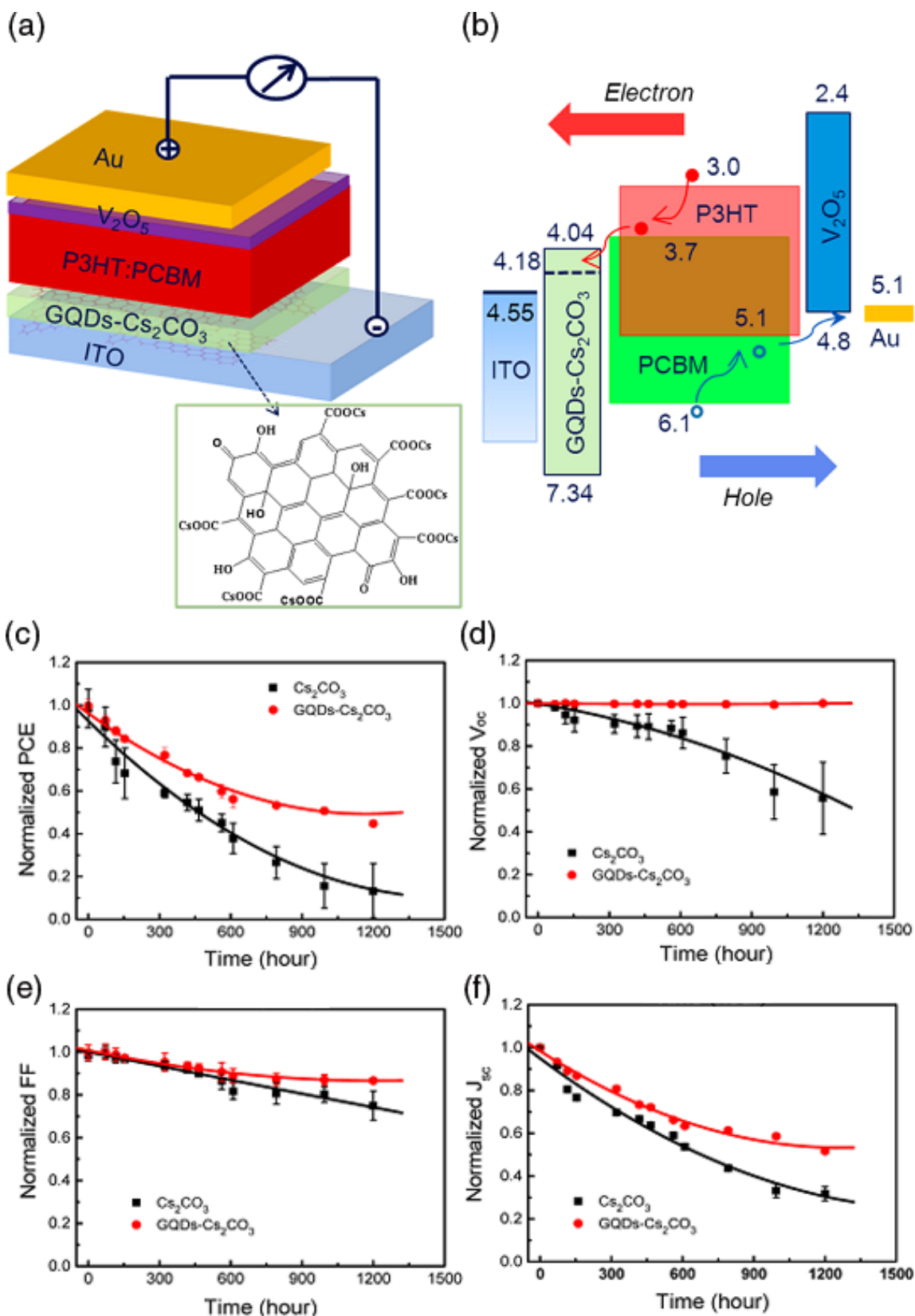


Figure 8. (a) Schematic of a graphene-based P3HT:PCBM solar cell structure containing GQDs- Cs_2CO_3 electron-selective layer, and (b) energy band diagram. The stability/degradation of solar cell parameters as a function of time; normalized (c) power conversion efficiency (PCE; η), (d) open-circuit voltage (V_{OC}), (e) fill factor (FF), and (f) photocurrent density (J_{SC}) of P3HT:PCBM inverted solar cells containing Cs_2CO_3 and GQDs- Cs_2CO_3 buffer, in air at room temperature and 65% relative humidity without encapsulation. Reprinted with permission from Ref. 127, H. B. Yang, Y. Q. Dong, X. Wang, S. Y. Khoo, and B. Liu, Cesium Carbonate Functionalized Graphene Quantum Dots as Stable Electron-Selective Layer for Improvement of Inverted Polymer Solar Cells, *ACS Appl. Mater. Interfaces*, 6, 1092–1099 (2014). Copyright © 2014 American Chemical Society.

In another study, Wang et al. [129] reported that the PCE of a PEDOT:PSS/PCDTBT:PC₇₁BM BHJ with interlayers of GO and GO/titanium oxide (TiO_x) as electron transport layers (ETLs) showed overall a 3% and 4% decay, respectively, after 30 days storage in air under ambient conditions. The PCDTBT:PC₇₁BM solar cell without an ETL showed a 56% decay in PCE over a period of 30 days under similar conditions. Average PCE and series resistance (R_s) of PEDOT:PSS/PCDTBT:PC₇₁BM-based solar cells without an ETL interlayer, with ETLs of TiO_x , GO, and GO/ TiO_x , were found to be 5.23%, 6.96%, 6.53%, and 7.45%, and $2.54 \Omega\text{cm}^2$, $2.50 \Omega\text{cm}^2$, $2.04 \Omega\text{cm}^2$, and $1.85 \Omega\text{cm}^2$, respectively. In the same study, P3HT:PCBM BHJ solar cells with an ETL layer of GO showed an 11% increased PCE value (3.29%) compared with a solar cell device without an ETL layer (PCE, 2.94%). Therefore, the insertion of a GO ETL contributes to long-term stability in BHJ devices. P3HT:PCBM-based

solar cells were fabricated by Jeon et al. [130] using conventional PEDOT:PSS as a HTL and compared with GO and moderately reduced GO as HTLs. The solar cell devices with thermally treated GO at 250 °C showed a PCE of 3.98% compared with a PCE of 3.85% for PEDOT:PSS as HTL. A similar trend was observed in stability in air where thermally treated GO-based devices were found to be superior in stability than PEDOT:PSS-based devices without encapsulation. The PCE of conventional PEDOT:PSS-based solar cells dropped to 0% after 10 h when exposed to air, whereas the PCE (3.98%) of solar cell devices having moderately reduced GO (referred to as thermally treated GO at 250 °C) as HTL remained at >70% in air after 48 h.

The stability of GO-based solar cells also has been evaluated. Chen et al. [131] used a rGO/GO composite, where rGO is 2 wt% of GO contents as the hole-collection material. (G002-GO denotes 2 wt% loading of rGO with respect to GO.) Figure 9 shows the current density-voltage ($J-V$) characteristics under illumination of solar cell devices containing GO, G002-GO, and PEDOT:PSS as hole-collection materials, and the variation of PCEs as a function of time for unencapsulated solar cells in ambient condition with 80% humidity. The PCEs of GO, G002-GO and PEDOT:PSS based solar cells were measured as 3.36, 4.21 and 4.04%, respectively. The series resistance (R_s) which influences the fill factor (FF) of solar cell devices was 11.29 $\Omega\cdot\text{cm}^2$ for GO which decreases to 3.82 $\Omega\cdot\text{cm}^2$ for G002-GO layer. The 4.04% PCE of the PEDOT:PSS device rapidly decreased to almost 0 after 8 h in ambient conditions with 80% humidity; however, the PCE of the rGO/GO-based solar cell remained at 73% of the original PCE value (4.21%) under the same conditions. The PCE of a solar cell increased from 3.36% for GO only to 4.21% for the rGO/GO composite-based device. The solar cell devices with rGO/GO showed higher PCEs and better stability resulting from the hydrophobic nature of rGO than for GO only.

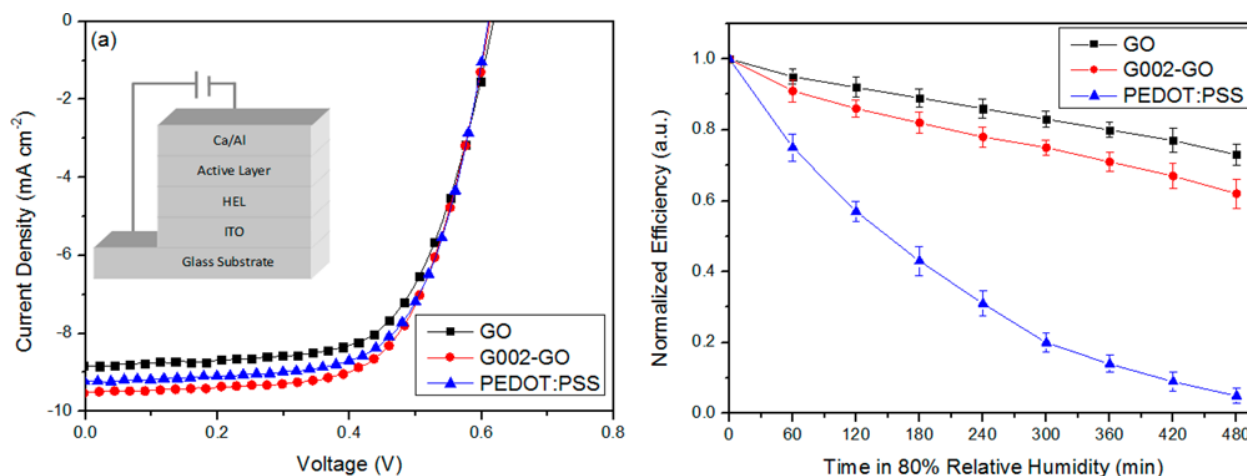


Figure 9. J - V characteristics under illumination of solar cells with GO, G002-GO, and PEDOT:PSS as hole-collection material, and the variation of PCEs as a function of time for unencapsulated solar cells in ambient condition with 80% humidity. Reprinted with permission from Ref. 131, L. Chen, D. Du, K. Sun, J. Hou, and J. Ouyang, Improved efficiency and stability of polymer solar cells utilizing two-dimensional reduced graphene oxide: Graphene oxide nanocomposites as hole-collection material, *ACS Appl. Mater. Interfaces*, 6, 22334–22342 (2014). Copyright © American Chemical Society.

For comparing stability, Kim et al. [132] fabricated GO containing P3HT:PCBM and P3HT:ICBA-based solar cell devices, which showed a trilayer of chemically modified GO as a good replacement for PEDOT:PSS, with excellent long-term stability. The GO-based ITO/ZnO:Cs₂CO₃/P3HT:ICBA/GO:PEDOT:PSS/Al solar cells showed a PCE of up to 3.70%, which decreased by 8.65 % over 4 weeks, while the control device lost 12.2% of PCE under similar conditions. An anode buffer layer of GO:PEDOT:PSS, which functions as an interlayer

material, provides not only higher PCEs, but also improved stability as a function of time when exposed to air.

Graphene and carbon nanotube composites have attracted significant attention for a synergetic approach. Li et al. [133] prepared a composite of carbon nanotube patched with graphene sheets. The composite films show flexibility, 90% optical transparency at 550 nm, with a R_s of 735 Ω/sq and a PCE of 5.2% for a CNTs/graphene/*n*-Si solar cell. Figure 10 shows the current density-voltage (*J-V*) curves and variations of photovoltaic parameters as a function of exposure time for CNTs/graphene-based solar cells and the schematic of carrier transport in a CNTs/graphene hybrid structure. The CNTs/graphene/*n*-Si solar cell showed a J_{sc} of 24.8 mA/cm^2 , a V_{oc} of 0.44 V, a fill factor (FF) of 24.6%, and a PCE of 2.7%. The solar cell devices were stored in air at room temperature. PCE gradually increased as a function of time and then stabilized at $\sim 4.5\%$ after a period of one week. There was no visible change in J_{sc} value during this time period except on day 7. Both V_{oc} and FF values increased to 0.53 V and 38%, respectively, resulting in an increase in PCE from 2.7% to 5.2% on day 8 due to the *p*-type doping by oxygen on exposure to air. The solar cell devices showed a PCE of 4% on day 12. High optical transparency and electrical conductivity of the CNTs/graphene composite film contribute to solar cell performance. The CNT acts as the conductive frame matrix, whereas the graphene sheets function as an intermediate layer that assists connection between the CNTs and *n*-Si layer, where CNTs/graphene composite film serves as a hole transporter.

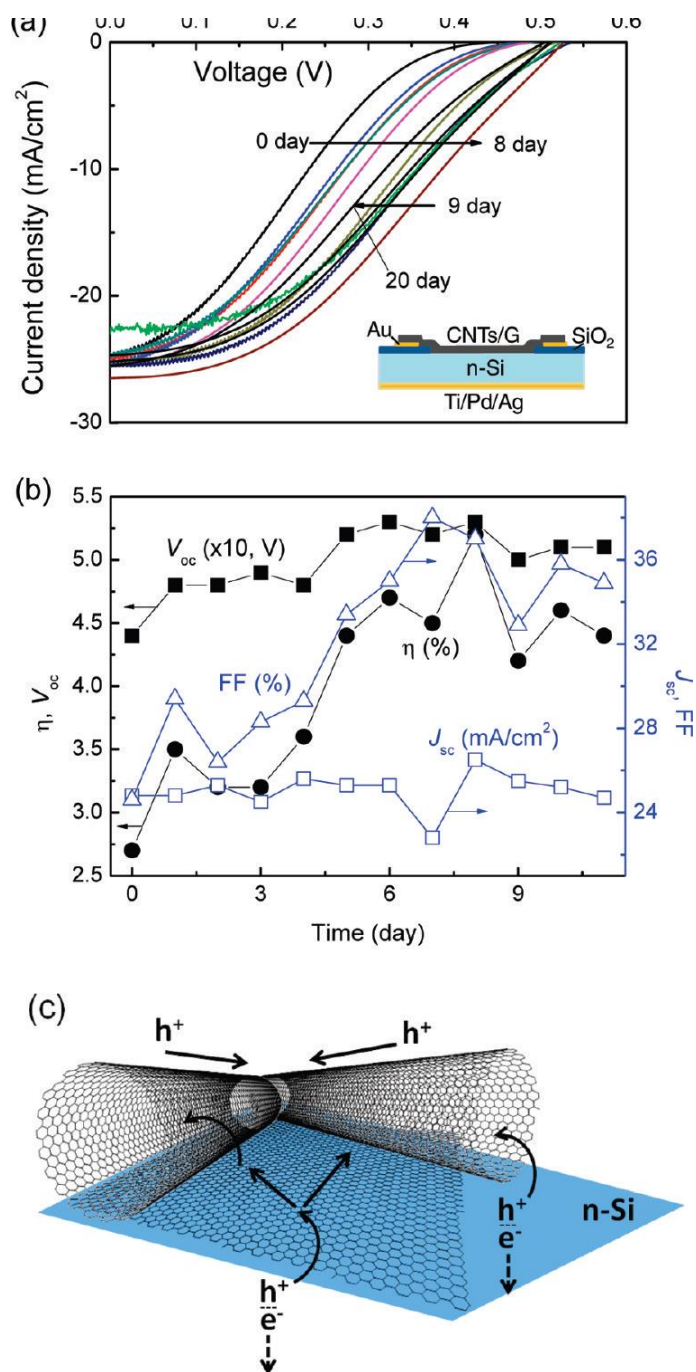


Figure 10. Photovoltaic properties of CNTs/graphene/ n -Si solar cells. (a) Light J - V curves, (b) Variation of photovoltaic parameters as a function of storage time, and (c) Schematic of carrier transport in the CNTs/graphene hybrid structure. Reprinted with permission from Ref. 133. C.

Li, Z. Li, H. Zhu, K. Wang, J. Wei, X. Li, P. Sun, H. Zhang, and D. Wu, Graphene Nano-“patches” on a Carbon Nanotube Network for Highly Transparent/Conductive Thin Film Applications, *J. Phys. Chem. C*, *114*, 14008–14012 (2010). Copyright © 2010 American Chemical Society.

TiO_x was used as an electron selective layer between the bottom electrode and the active layer for fabricating inverted solar cell devices with GO as anode layer [134]. The TiO_x-based solar cell devices showed enhanced PCE compared with solar cells without TiO_x. This indicates that TiO_x effectively acted in blocking holes at the interface of the active and bottom layers. The solar cells showed a 3.67% decrease in PCE after 2160 h (90 days) of storage, hence the solar cells were very stable because no PEDOT:PSS blend was used. Kim et al. [135] used spin-coated rGO films as an anode buffer layer in constructing BHJ solar cell devices with a photoactive layer consisting of [poly({4,8-di(2-ethylhexyloxy)benzo[1,2-b:4,5-b']dithiophene}-2,6-diyl)-*alt*-({5-octythieno[3,4-c]pyrrole-4,6-dione}-1,3-diyl):fullerene (PBDTTPD:PCBM) blends. Both J_{sc} and fill factor (FF) increased after the rGO buffer layer was added, which increased PCE to 4.8%, and which remained above 70% after 4 weeks. Figure 11 shows the changes in normalized PCE as a function of storage time for solar cell devices without GO, with rGO, with GO, and with PEDOT:PSS layers. Solar cell devices without GO and with PEDOT:PSS degraded rapidly while solar cell devices with a GO buffer layer showed the best stability compared to those with a rGO layer.

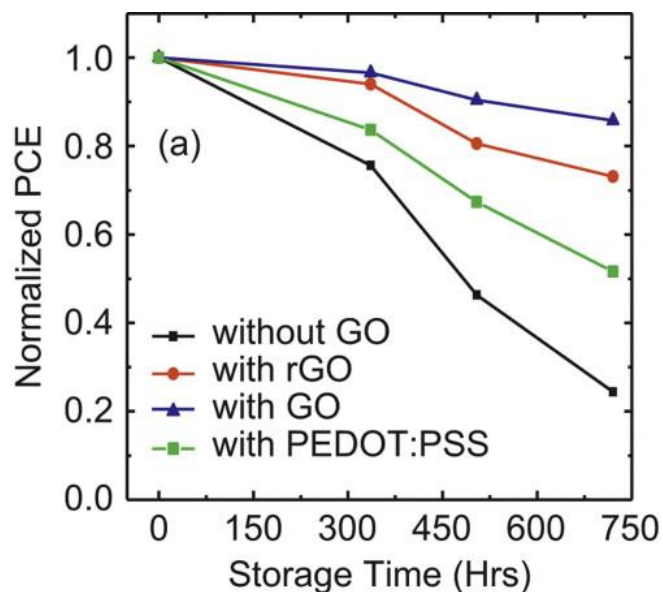


Figure 11. Normalized PCE as a function of storage time for solar cell devices without GO, with rGO, with GO, and with PEDOT:PSS. Reprinted with permission from Ref. 135, H. P. Kim, A. R. bin Mohd Yusoff, and J. Jang, Organic solar cells using a rGO anode buffer layer, *Solar Energy Materials and Solar Cells*, 110, 87–93 (2013). Copyright © 2013 Elsevier.

Gold nanoparticles (AuNPs) also have been used for enhancing photovoltaic properties and stability in organic solar cells. Stratakis et al. [136] studied the stability of BHJ solar cells having GO as a HTL and AuNPs between the photoactive and GO layers. The PCEs of 2.86%, 2.90%, and 3.37% were measured for PEDOT:PSS, GO, and GO/AuNPs-based devices, respectively. The plasmonic GO-based solar cell devices ITO/GO/AuNPs/P3HT:PCBM/Al showed a 30% enhancement compared to PEDOT:PSS layer-based devices. From a stability point of view, GO-based devices retained 50% of their initial PCE value after continuous illumination for 45 h, whereas the PEDOT:PSS-based devices failed after 20 h. The photovoltaic performance is

associated with AuNPs-induced plasmonic absorption enhancement. The enhancement in stability may be due to the limited oxygen and indium diffusion from the ITO electrode into the photoactive layer. A 3-layer graphene/PEDOT: PSS/*n*-Sn solar cell showed a PCE of 5.48%, which decreased to 4.84% after one month, while the PCE of an ITO-based device decreased from 5.38% to 4.16% over the same period of time, as reported by Li et al. [137]. The PCE of a 3-layer graphene/PEDOT:PSS/*n*-Si hybrid solar cell device decreased by 11.7% over a period of one month compared to a 22.7% decrease in an ITO electrode-based solar cell under similar conditions.

Graphene quantum dots (GQDs) also have been used in the fabrication of solar cells. Gao et al. [138] developed GQDs-based heterojunction solar cells with H-, SiO_x-, and CH₃- terminal groups on a silicon surface. The CH₃-Si/GQDs devices showed the highest PCE of 6.63%, compared to PCEs of 2.24% for H-Si/GQDs and 2.92% for SiO_x-Si/GQDs-based solar cell devices. The CH₃-Si/Au control device had a PCE of 2.26% without a GQDs layer. The PCE was found to be dependent on GQD layer thickness and on the size of the GQDs. Figure 12 shows stability/degradation of the CH₃-Si/GQD heterojunction solar cell devices in terms of open-circuit voltage (*V*_{oc}), short-circuit photocurrent density (*J*_{sc}), fill factor (FF), and PCE as a function of time after storing for 180 days in a nitrogen (N₂)-filled glovebox without any encapsulation. Both *V*_{oc} and FF values remained unchanged for up to 180 days, whereas the short-circuit photocurrent density (*J*_{sc}) value degraded from 28.71 mA/cm² to 22.35 mA/cm², and the PCE decreased from 6.35% to 5.15%. The changes in both *J*_{sc} and PCE could be due to the gradual chemical degradation of silicon-surface CH₃- terminal groups as a function of storage time.

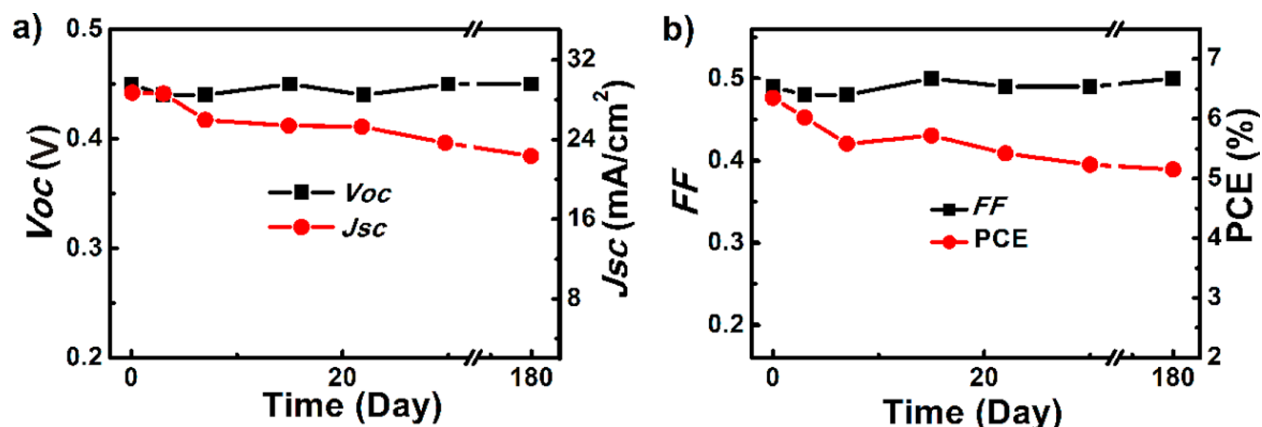


Figure 12. Stability/degradation of $\text{CH}_3\text{-Si/GQD}$ heterojunction solar cell devices as a function of time after storing in a nitrogen (N_2)-filled glove-box without any encapsulation: (a) open-circuit voltage (V_{oc}) and short-circuit photocurrent density (J_{sc}), and (b) fill factor (FF) and PCE. Reprinted with permission from Ref. 138, P. Gao, K. Ding, Y. Wang, K. Ruan, S. Diao, Q. Zhang, B. Sun, and J. Jie, Crystalline Si/Graphene Quantum Dots Heterojunction Solar Cells, *J. Phys. Chem. C* 118, 5164–5171 (2014). Copyright © American Chemical Society.

6. Approaches to Improve Stability of Organic Solar Cells

The failure of organic solar cells can occur due to the chemical degradation of materials by oxygen and moisture contaminations, ultraviolet light exposure, high temperature, corrosion of electrodes, interconnect and interfacial breakage due to the PEDOT:PSS interfacial layer [89-102]. The degradation can lead to increase in series resistance, loss in optical transparency and overall photovoltaic performance of solar cell devices. Therefore, long-term performance of organic solar cells under atmospheric conditions is of critical importance for commercial applications. The long-term stability of organic BHJ solar cells under different atmospheric conditions can be improved by interfacial buffer layer [139], encapsulation [140-142], UV

absorbing film [143], crosslinker [144], and other approaches [145-147]. For example, encapsulation can protect solar cells from humidity, oxygen, and other chemicals present in an external environment. Po et al. [148] analyzed the role of buffer layers in polymer solar cells. The problems associated with stability/degradation of organic and polymer solar cells can be addressed by using buffer layers of fullerene and lithium fluoride interlayers [149], transition metal oxides [150], and titanium suboxide [146, 151, 152]. Both MoO₃ and ZnO buffer layers in inverted solar cell devices were found to improve stability [153], and likely, thermal annealing under vacuum also led to higher stability for organic solar cells [154]. Kesters et al. [155] suggested the enhancement of stability in organic solar cells by polymer (PCPDTBT) side chain functionalization. Peters et al. [156] estimated the average lifetime for a poly[N-9-heptadecanyl-2,7-carbazole-alt-5,5-(4,7-di-2-thienyl-2,1,3-benzothiazole)] (PCDTBT) containing BHJ solar cell device (ITO)/poly(3,4-ethylenedioxythiophene) (PEDOT:PSS)/PCDTBT:PC₇₀BM/Ca/Al to be more than 6 years, twice that of a poly(3-hexylthiophene) (P3HT)-based solar cell device at 5.5 hours of one-sun intensity per day for a whole year. Kong et al. [157] pointed to burn-in loss, leading to degradation, as one of the main factors in the short life span of polymer-based solar cells. The initial burn-in loss was decreased by separating pristine photoactive polymers and trap-embedded components using the molecular weight distributions, which resulted in enhanced PCE and long-term stability of polymer solar cells without sudden initial burn-in degradation. As discussed earlier, several approaches have been applied toward improving the stability of organic solar cells. In addition to other factors, the influence of water and moisture on the photovoltaic performance and stability is of major concern for organic solar cells [158-163]. CORDIS European Union estimated a 1 billion Euros market for roll-to-roll mass-produced organic solar

cells by 2016, and launched the ESTABLIS program to ensure long-term stability in organic solar cell devices [164].

7. Use of Graphene-Based Materials in Improving Stability of BHJ Solar Cells

Graphene-based materials have been widely used for solar cell applications, as noted. Graphene-based solar cells show better photovoltaic performance and stability than PEDOT:PSS-based solar cell devices. Only limited data on the stability of graphene-based solar cells are available in the literature; these have been summarized in this article. The use of different inorganic semiconductors with graphene has been explored. Tongay et al. [165] studied thermal stability of graphene/GaN interfaces using Raman Spectroscopy and current-voltage measurements at high temperatures. The Schottky barriers between GaN and graphene were stable up to 550 K which became non-rectifying over 650 K, however the rectification was recovered upon cooling.

The chemical functionalization of graphene-based materials has been evaluated for solar cell devices. Stratakis et al. [166] developed an ultraviolet laser irradiation-based photochemical method for simultaneous partial reduction as well as doping of GO ultrathin films in the presence of a chloride precursor gas. The chlorinated GO-Cl films were characterized by Raman and XPS techniques to confirm grafting of chloride molecules to the edges and the basal plane of GO film. Both the doping and reduction levels of GO was controlled by laser exposure time, and therefore the work function of the chlorinated GO-Cl layers was modified from 4.9 eV to 5.23 eV. The polymer donors, P3HT with a HOMO level of 5.0 eV and PCDTBT with a HOMO level of 5.3 eV, were used to examine the effect of the GO and the work function on the photovoltaic properties. The PCDTBT:PC₇₁BM-based solar cell devices containing GO-Cl as a hole transporting layer (HTL) showed a PCE of 6.56% compared to a PCE of 5.59% for pristine GO-

based devices, and 5.49% for PEDOT:PSS-based solar cell devices. The PCE of P3HT:PC₆₁BM-based solar cell devices containing GO-Cl as HTL was 3.74%, also higher than PCEs of 3.28% for the pristine GO HTL and 3.23% for the PEDOT:PSS HTL-based solar cell devices. The higher PCE occurred from efficient hole transportation as a result of the energy level matching between the polymer donor and GO-Cl. The hole mobility was found to increase with increasing work function of the GO-Cl. The solar cell devices based on GO showed significantly higher stability under continuous solar illumination in air compared to PEDOT:PSS-based devices without any encapsulation. PEDOT:PSS-based solar cells failed after 20 h, whereas the solar cells fabricated with pristine GO or where GO was the HTL retained over 70% and 50% of their initial PCE values for over 25 h and 45 h, respectively. Such a degradation occurs because of the highly acidic nature of the spin-coated PEDOT:PSS layer, which causes corrosion of the ITO electrode, as well as indium migration into the photoactive layers. GO as HTL enhances both the PCE of solar cell devices, as well as their stability.

In another study, Kakavelakis et al. [167] used lithium-neutralized graphene oxide (GO-Li) as an interlayer between the photoactive layer and the metal oxide electron-transporting layer (ETL) in poly[N-9-heptadecanyl-2,7-carbazole-alt-5,5-(4,7-di-2-thienyl-2,1,3-benzothiazole)] (PCDTBT):[6,6]phenyl C₇₁ butyric acid methyl ester (PC₇₁BM)-based solar cell devices. Figure 13 shows the *J-V* characteristics and schematic illustration of the PCDTBT:PC₇₁BM devices with TiO_x, GO/ TiO_x, and GO-Li/ TiO_x as the ETL and functionalization with Li alkali metal. The insertion of a GO-Li interlayer resulted in a superior interface between the ETL and the photoactive layer. The work function of 4.30 eV for GO-Li perfectly matches the LUMO level of the fullerene-based acceptor material to enhance electron extraction. PCDTBT:PC₇₁BM-based solar cell devices with a GO-Li layer showed a significant increase in the PCE, from 5.51% for

TiO_x to 6.29% for GO-Li/TiO_x as the ETL, a 14.2% enhancement over solar cell devices without the graphene-based interfacial layer. PCE values of 5.71%, 6.29%, and 4.84% were measured for GO-Li/TiO_x-based devices for 1.3-nm, 2.0-nm, and 3.1-nm thickness, respectively, showing the effect of different GO-Li thickness on PCE values. The insertion of the GO-Li as an interfacial layer also increased the electron mobility of the device, which resulted in increased *J*_{sc} and a decrease in contact resistance from 18.18 Ω for the TiO_x as the ETL to 16.95 Ω for the GO-Li/TiO_x as the ETL. The GO-Li devices also showed higher stability compared to devices without an interlayer because the GO-Li layer acts as a moisture and oxygen diffusion barrier, leading to long-term stability for the solar cell devices. The PCDTBT:PC₇₁BM/TiO_x device lost 42% of its initial PCE value after continuous solar illumination for 24 h, whereas the PCDTBT:PC₇₁BM/GO-Li/TiO_x solar cell device retained 56% of its initial PCE value under similar conditions. The degradation rate was found to be saturated after 100 h of continuous solar illumination for both solar cell devices. The single-layer TiO_x ETL device exhibited 27% of its initial PCE value compared to 35% of initial PCE value for a bilayer GO-Li/TiO_x as the ETL, which indicates improved stability. In addition to the role of ETL in increasing PCE, the GO-Li interlayer also serves as a protecting layer against humidity and oxygen, thereby enhancing stability under prolonged solar illumination.

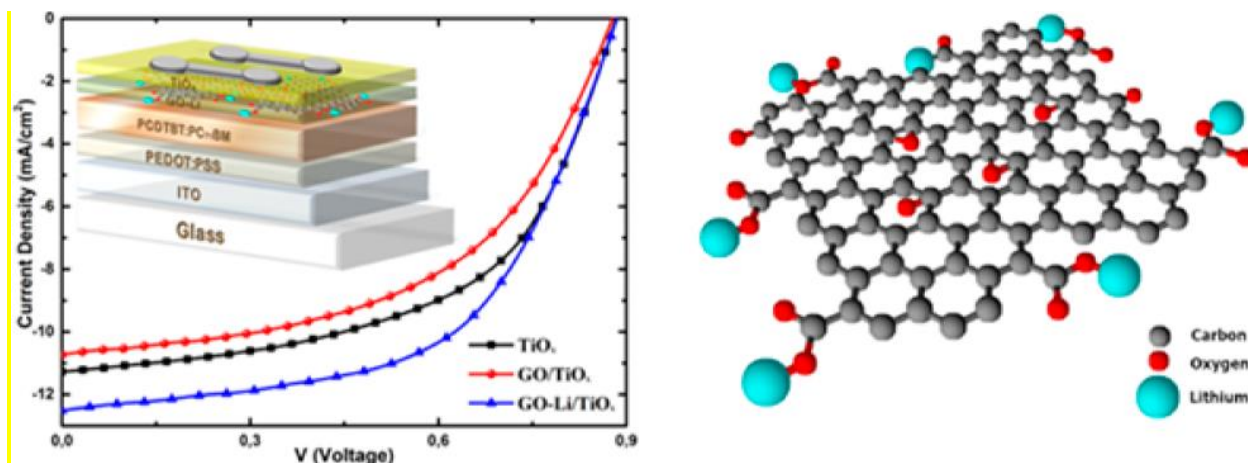


Figure 13. J - V characteristics and schematic illustration of the PCDTBT:PC₇₁BM devices with TiO_x, GO/TiO_x, and GO-Li/TiO_x as the ETL and functionalization with Li alkali metal. Reprinted with permission from Ref. 167, G. Kakavelakis, D. Konios, E. Stratakis, and E. Kymakis, Enhancement of the efficiency and stability of organic photovoltaic devices via the addition of a lithium-neutralized graphene oxide electron-transporting layer, *Chem. Mater.* 26, 5988-5993 (2014). Copyright © American Chemical Society.

The gas-barrier properties of graphene-based materials have been examined for device applications. Bunch et al. [168] reported that a single layer of graphene membrane has unique separation barrier properties and is impermeable to helium. This gas barrier property of graphene was applied to improve the stability of organic solar cell devices. Kim et al. [169] used rGO-based thin films as gas barriers to improve the stability of organic P3HT:PC₆₀BM and poly[N-9-heptadecanyl-2,7-carbazole-alt-5,5-(4,7-di-2-thienyl-2,1,3-benzothiazole)] (PCDTBT):PC₇₀BM solar cell devices in ambient air. The P3HT:PC₆₀BM and PCDTBT:PC₇₀BM solar cell devices

were encapsulated by rGO thin film using spin-casting of GO suspension onto an Al electrode. For GO-encapsulated devices, thermal annealing was done at 150 °C for 30 min before the spin-casting of the GO layer, while for rGO-encapsulated devices, thermal annealing was performed after the spin-casting of the GO layer. The rGO layers were achieved after the thermal annealing of the GO-covered solar cell devices at 150 °C for 30 min. Large-flake graphite is denoted as GO(L). The average initial PCEs of GO(L)-encapsulated, rGO(L)-encapsulated P3HT:PC₆₀BM solar cell devices, and a non-encapsulated reference device were 2.85%, 2.85%, and 2.82%, which decreased to 0.07%, 2.39%, and 0.04% after 6 h storing in ambient air, respectively. This shows that large-flake rGO film enhances stability and protects the solar cell devices against water vapors, while GO films do not provide such protection in enhancing stability. Large-flake rGO films have superior gas barrier properties due to the increased length of the diffusion path of water molecules and high dispersibility of GO(L) in suspension. Figure 14 shows performance stabilities under ambient conditions of P3HT:PC₆₀BM solar cell devices without and with rGO(L) encapsulation, *J-V* characteristics of the P3HT:PC₆₀BM solar cell after different exposure times from 0 h to 560 h, as well as with GO(L) and rGO(L, sonic) encapsulations from 0 h to 120 h. The rGO(L, sonic)-based film showed better stability of solar cell devices compared with rGO(L) film. The lifetime of the rGO(L, sonic)-encapsulated solar cell devices was increased 50 times over that of a reference device. This also demonstrates that the high dispersibility from sonication leads to better gas-barrier properties. The PCEs of PCDTBT:PC₇₀BM inverted devices encapsulated with polyethylene naphthalate (PEN)/rGO films also were examined and showed an 8% decrease in PCE after 24 h storing at 100% relative humidity. The PCDTBT:PC₇₀BM inverted solar cell devices retained 43% of their original PCEs after 240 h (10 days). Thermal reduction of GO film at a low heating rate yielded lower water

vapor permeability, which was 0.1% compared with PEN film. It was found that surface roughness, dispersibility, and reduction conditions of a GO film significantly affect the gas-barrier performance. A GO solution prepared from large-flake graphite was found to show high dispersibility and to produce rGO thin film with superior gas-barrier properties. Thermal reduction conditions of GO films also influenced the water vapor permeability of rGO films prepared on a flexible substrate where slow heating led to low surface roughness, a small surface area, and therefore lower water vapor permeability. The study shows that the stability of both P3HT:PC₆₀BM and PCDTBT:PC₇₀BM solar cell devices was significantly improved using rGO as a gas-barrier film.

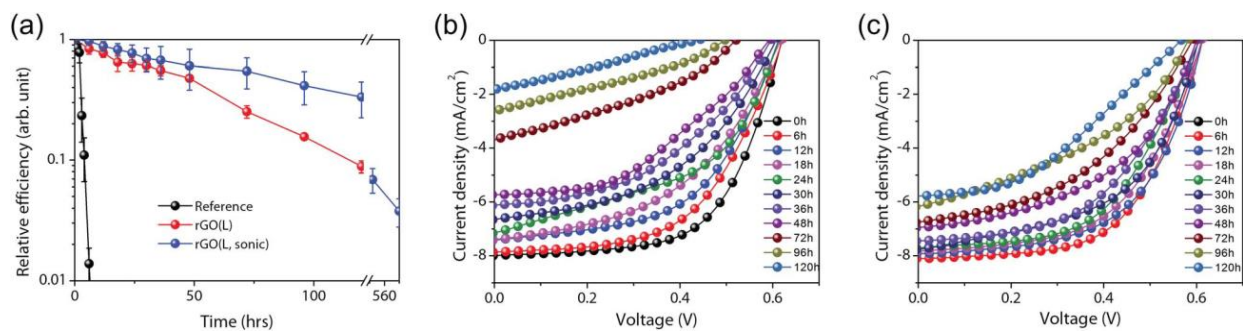


Figure 14. (a) Performance stabilities under ambient conditions of P3HT:PC₆₀BM solar cell devices without encapsulation and with rGO(L) encapsulation. J - V characteristics of the P3HT:PC₆₀BM solar cell after different exposure times: (b) with GO(L) encapsulation, and (c) with rGO(L, sonic) encapsulation. Here the large-flake graphite is denoted as GO(L); fragmented GO in the sonicated suspension is referred to as GO(L, sonic). Reprinted with permission from Ref. 169, T. Kim, J. H. Kang, S. J. Yang, S. J. Sung, Y. S. Kim, and C. R. Park, Facile preparation of reduced graphene oxide-based gas barrier films for organic photovoltaic devices, *Energy Environ. Sci.*, 7, 3403-3411 (2014). Copyright © Royal Society of Chemistry.

Graphene-based materials have been used as surface coating for studying their protective effect on solar cell devices. Ahn et al. [170] developed a copper nanowire–graphene (CuNW-G) core–shell nanostructure using plasma-enhanced CVD process at 400 °C. The CuNW-G core–shell nanostructure was characterized by X-ray photoelectron spectroscopy, X-ray diffraction, scanning electron microscopy, transmission electron microscopy, and Raman spectroscopy. The CuNW-G core–shell nanostructure–based transparent conducting electrode (TCE) showed better optical and electrical properties compared to an ITO electrode, as well as excellent thermal oxidation and chemical stability due to the encapsulation of the CuNW by gas-impermeable graphene shells. The optical transmittance and sheet resistance of the CuNW and CuNW-G based TCEs were found to be 79.8% and 79.0% at 550 nm and 32 and 36 k Ω /sq, respectively. The CuNW and CuNW-G core shell nanostructures were used as anode layers in fabricating BHJ polymer solar cell structure of CuNW or CuNW-G/PEDOT:PSS/PTB7:PC₇₁BM/LiF/Al. The BHJ PSC with CuNW-G–based BHJ solar cells showed a PCE of 4.04%, a short-circuit current density (J_{sc}) of 8.20 mA cm⁻², an open-circuit voltage (V_{oc}) of 0.73 V, and a fill factor (FF) of 67.8%. The control BHJ solar cell device with CuNW exhibited a PCE of 1.90%, J_{sc} of 10.84 mA cm⁻², V_{oc} of 0.73 V, and a FF of 24.1%. Therefore, CuNW-G based solar cells have higher photovoltaic performance than CuNW devices. The gas-barrier effect of the graphene shell was examined. The thermal oxidation stability of the CuNW and CuNW-G–based TCEs were studied in ambient conditions for 30 days by monitoring variations in the sheet resistance (Figure 15). The sheet resistance of the CuNW-based TCE remarkably increased by 1800 times within 2 days. On the other hand, the sheet resistance of the CuNW-G–based TCE showed a slight

increase after 30 days. When CuNW-based TCEs were exposed to higher temperature and humidity (70 °C/70% RH) conditions, the sheet resistance increased by 76 times within 30 min whereas the sheet resistance of the CuNW-G-based TCEs slightly increased by 27% after 120 h. The highly improved thermal oxidation stability of the CuNW-G-based TCEs clearly indicates that the graphene shell induces long-term stability for the CuNW core. Figure 16 shows SEM images of CuNW/PEDOT:PSS and CuNW-G/PEDOT:PSS films after 1 hr of PEDOT:PSS coating. A few CuNWs were oxidized due to the acidic nature of the PEDOT:PSS coating, causing a dramatic reduction in electrical properties. The CuNW-G-based TCE exhibits excellent chemical resistance against PEDOT:PSS acidic corrosion, demonstrating the chemical inertness of the graphene shell against acidic conditions. Therefore, improved chemical stability of a CuNW-G-based TCE results in an enhanced PCE in solar cell devices. The improved oxidation stability of a CuNW-G nanostructure over CuNW was also confirmed under harsh conditions by dispersing in deionized (DI) water for 1 day. The CuNW-G solution showed no noticeable color change, indicating the graphene shell provides protection to the CuNW core against oxidation. The CuNW changed in color from red to black due to copper oxide formation. The sheet resistance of the CuNW-based TCE after DI water treatment was found to be 125 times higher compared to CuNW without DI water treatment, whereas the sheet resistance of the CuNW-G-based TCE remained the same regardless of DI water treatment. This study confirms that the CuNW-G core-shell nanostructure provides superior oxidation stability due to the excellent moisture and gas-barrier property of graphene.

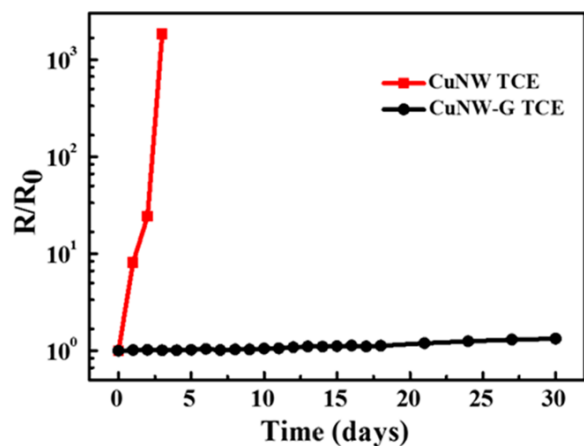


Figure 15. The variation of sheet resistance of CuNW and CuNW-G-based TCEs in air at room temperature for 30 days during a stability test. Reprinted with permission from Ref. 170, Y. Ahn, Y. Jeong, D. Lee, and Y. Lee, Copper nanowire–graphene core–shell nanostructure for highly stable transparent conducting electrodes, *ACS Nano* 9, 3125-3133 (2015). Copyright © American Chemical Society.

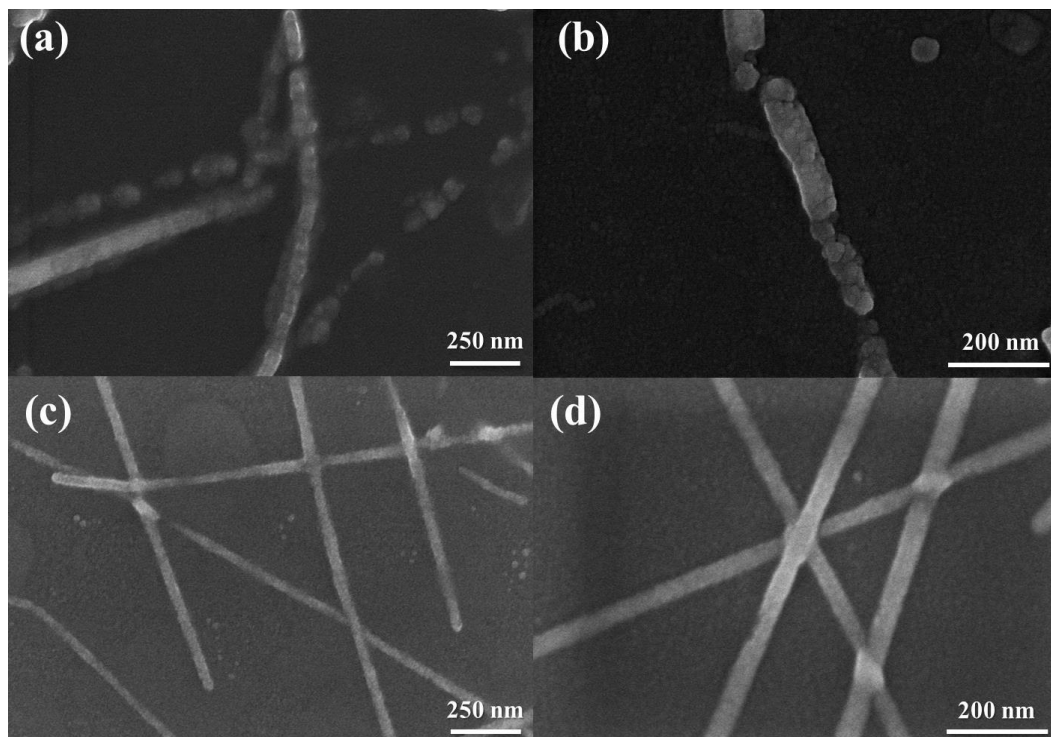


Figure 16. SEM images of CuNW/PEDOT:PSS films (a) and (b), and CuNW-G/PEDOT:PSS films (c) and (d), after 1 hr of PEDOT:PSS coating. Reprinted with permission from ref. 170, Y. Ahn, Y. Jeong, D. Lee, and Y. Lee, Copper nanowire–graphene core–shell nanostructure for highly stable transparent conducting electrodes, *ACS Nano* 9, 3125-3133 (2015). Copyright © American Chemical Society.

Other approaches have been utilized to introduce stability in graphene-based BHJ solar cells. Yeo et al. [171] prepared sulfonic acid groups–functionalized graphene oxide (sr-GO), which show good compatibility with various HOMO materials. The sr-GO-based solar cells showed PCEs over 7% and superior stability over PEDOT:PSS-based solar cell devices. Kim et al. [172] used microwave-assisted reduced graphene oxide (M-rGO) as a hole extraction layer (HEL) with PEDOT:PSS in BHJ solar cells. The M-rGO-based solar cell showed a PCE of 3.57%, 21% higher than that PEDOT:PSS HEL–based devices. The PCE of PEDOT:PSS-based solar cells completely degraded after 1000 h in atmospheric condition without any encapsulation, whereas MR-GO-based solar cells retained over 85% of initial PCE value. The M-rGO interfacial layer provided a long-term stability to solar cells after storing in atmospheric conditions. Sapkota et al. [xx] demonstrated a significant improvement in the stability of encapsulated BHJ solar cells using layer configuration of Cr/Al/Cr/P3HT:PCBM/PEDOT:PSS/metal under different aging conditions. The flexible solar cell devices retained >95% of their initial PCE after 1000 h of aging at 85 °C under 85% relative humidity. The encapsulated solar cell devices between two

glass plates retained over 90% of their initial PCE over 1800 h of aging under similar conditions. The Cr/Al/Cr/P3HT:PCBM/PEDOT:PSS/metal devices, when encapsulated between two glass plates as well as between a glass plate and flexible barrier film, exhibited no degradation over 10,000 h at 85 °C in dark and ambient air. Only a 10% decrease in photovoltaic performance was noticed after 12,000 h under continuous illumination of 1000 W/m². This study showed promising long-term stability for encapsulated BHJ organic solar cells.

It has become evident from above studies that the insertion of graphene-based materials either as thin film or layer in solar cell devices does help in stopping degradation and enduring environmental stability. Graphene layers in solar cell devices perform equivalent to other approaches of encapsulation and buffer materials. Graphene does prevent diffusion at the interfaces of interlayer/electrode. Graphene inherently acts as a barrier to water and moisture. Approaches similar to those used to fabricate organic solar cells can be applied to graphene-based hybrid BHJ solar cells to prevent their degradation and to further improve their long-term stability. The long-term stability and degradation of graphene-based solar cells is one of several critical, challenging tasks for the scientific community in the development of these photovoltaic devices. Long-term pilot studies like organic and polymer solar cells should be conducted to evaluate the feasibility of graphene-based BHJ solar cells for commercial purposes.

8. Conclusion and Perspective

The photovoltaic data on stability of different types of graphene-based heterojunction solar cell devices were discussed in reference to organic solar cells. It is clearly evident from above summarized data that when graphene-based materials were used as a buffer layer or as replacement material in solar cell structures, the stability was significantly improved. For

example: (1) P3HT:PCBM-based solar cells with GO as a buffer layer showed significantly superior stability in air compared to conventional PEDOT:PSS blend-based solar cells [110], (2) solar cells with a spin-coated GO buffer layer on an ITO electrode exhibited significantly enhanced stability and a prolonged lifetime of solar cells compared to bare ITO-based devices [113], and (3) when applying GO or GO/TiO_x as electron transport layers (ETLs) in PEDOT:PSS/PCDTBT:PC₇₁BM bulk heterojunction solar cell devices, PCE showed only a 3-4% decay compared to a 56% decay without ETL after 30 days in air; the degradation of solar cells was significantly reduced [129]. Graphene-based materials such as graphene oxide (GO), reduced GO and graphene itself offer great potential for the further improvement not only of solar cell photovoltaic performance but also long-term environmental stability against chemicals and photo-oxidation. The graphene/*n*-Si heterojunction solar cells show superior performance in terms of achieving higher power conversion efficiency and stability and degradation in comparison with other graphene-based organic solar cell devices based on conducting polymer blends. There are still many challenges in the field of graphene-based solar cells from achieving high power conversion efficiency to cost-effective production to enduring better environmental stability which should be addressed for commercial applications. The toxicity of nanostructured materials is well known [174,175], and the degradation caused by toxicity could be a point of concern. Graphene-based materials may cause cytotoxicity to humans [176-181]. Therefore, in addition to stability and degradation, such issues should also be addressed. The main objective is to find low-cost graphene materials based solar cells with high efficiency. Current ITO based solar cells are expensive and future availability is of concern, therefore, graphene-based materials have emerged as a potential replacement but overall cost depends upon the large-scale production and ease of processability. The graphene-based materials offer both easy solution

processability and scalability. The lifetime of graphene-based solar cells has been studied from a few hours to 3 months. The preserving lifetime of at least 4-5 years for graphene-based solar cells is desirable to be used for commercial applications.

Disclaimer

The details contained in this review article are for information purposes only. The authors, editors, and publisher cannot accept liability of any kind whatsoever for the accuracy of content and data, any omissions or errors, or a claim of completeness.

References (*Authors wish to keep research article titles and starting-ending page numbers as such in all references if possible*)

1. T. Saga, Advances in crystalline silicon solar cell technology for industrial mass production, *NPG Asia Materials* 2, 96–102 (2010)
2. (a) E. D. Dunlop and D. Halton, The performance of crystalline silicon photovoltaic solar modules after 22 years of continuous outdoor exposure, *Progress in Photovoltaics: Research and Applications* 14, 53–64 (2006); (b) D. C. Jordan and S. R. Kurtz, Photovoltaic degradation rates—an analytical review, *Progress in Photovoltaics: Research and Applications* 21, 12-29 (2013)
3. Z. He, C. Zhong, S. Su, M. Xu, H. Wu and Y. Cao, Enhanced power-conversion efficiency in polymer solar cells using an inverted device structure, *Nature Photonics*, 6, 591-592 (2012)
4. S. H. Liao, H.-J. Jhuo, P.-N. Yeh, Y.-S. Cheng, Y.-L. Li, Y.-H. Lee, S. Sharma, and S.-A. Chen, Single Junction Inverted Polymer Solar Cell Reaching Power Conversion Efficiency

- 10.31% by Employing Dual-Doped Zinc Oxide Nano-Film as Cathode Interlayer, *Scientific Reports* 4, Article number 6813 (2014). doi:10.1038/srep06813
5. J. You, L. Dou, K. Yoshimura, T. Kato, K. Ohya, T. Moriarty, K. Emery, C. C. Chen, J. Gao, G. Li and Y. Yang, A polymer tandem solar cell with 10.6% power conversion efficiency. *Nature Commun.* 4, 1446–1455 (2013).
6. L. Huo, T. Liu, X. Sun, Y. Cai, A. J. Heeger, and Y. Sun, Single-Junction Organic Solar Cells Based on a Novel Wide-Bandgap Polymer with Efficiency of 9.7%, *Adv. Mater.* 27, 2938-2944 (2015)
7. S.-H. Liao, H.-J. Jhuo, Y.-S. Cheng, and S.-A. Chen, Fullerene Derivative-Doped Zinc Oxide Nanofilm as the Cathode of Inverted Polymer Solar Cells with Low-Bandgap Polymer (PTB7-Th) for High Performance, *Adv. Mater.*, 25, 4766-4771 (2013)
8. H. Zhou, Y. Zhang, C.-K. Mai, S. D. Collins, G. C. Bazan, T.-Q. Nguyen, and A. J. Heeger, Polymer Homo-Tandem Solar Cells with Best Efficiency of 11.3%, *Adv. Mater.* 27, 1767-1773 (2015)
9. M. Jørgensen, K. Norrman, and F. C. Krebs, Stability/degradation of polymer solar cells, *Solar Energy Materials and Solar Cells* 92, 686-714 (2008)
10. M. Jørgensen, K. Norrman, S. A. Gevorgyan, T. Tromholt, B. Andreasen and F. C. Krebs, Stability of polymer solar cells, *Adv. Mater.*, 24, 580–612, (2012)
11. N. Grossiord, J. M. Kroon, R. Andriessen, and P. W. M. Blom, Degradation mechanisms in organic photovoltaic devices, *Organic Electronics* 13, 432-456 (2012)
12. M. Manceau, A. Rivaton, J.-L. Gardette, S. Guillerez, and N. Lemaître, Light-induced degradation of the P3HT-based solar cells active layer, *Solar Energy Materials and Solar Cells* 95, 1315-1325 (2011)

13. T. Tromholt, M. Manceau, M. Helgesen, J. E. Carlé, and F. C. Krebs, Degradation of semiconducting polymers by concentrated sunlight, *Solar Energy Materials and Solar Cells* 95, 1308-1314 (2011)
14. H. Cao, W. He, Y. Mao, X. Lin, K. Ishikawa, J. H. Dickerson, and W. P. Hess, Recent progress in degradation and stabilization of organic solar cells, *J. Power Sources* 264, 168-183 (2014)
15. A. Guerrero, P. P. Boix, L. F. Marchesi, T. Ripolles-Sanchis, E. C. Pereira, and G. Garcia-Belmonte, Oxygen doping-induced photogeneration loss in P3HT: PCBM solar cells, *Solar Energy Materials and Solar Cells* 100, 185-191 (2012).
16. M. Wang, F. Xie, J. Du, Q. Tang, S. Zheng, Q. Miao, J. Chen, N. Zhao, and J. B. Xu, Degradation mechanism of organic solar cells with aluminum cathode, *Solar Energy Materials and Solar Cells* 95, 3303-3310 (2011)
17. K. Norrman, M. V. Madsen, S. A. Gevorgyan, and F. C. Krebs, Degradation patterns in water and oxygen of an inverted polymer solar cell, *J. Am. Chem. Soc.* 132, 16883-16892 (2010).
18. R. Roesch, K.-R. Eberhardt, S. Engmann, G. Gobsch, and H. Hoppe, Polymer solar cells with enhanced lifetime by improved electrode stability and sealing, *Solar Energy Materials and Solar Cells* 117, 59-66 (2013)
19. S. A. Gevorgyan, A. J. Medford, E. Bundgaard, S. B. Sapkota, H.-F. Schleiermacher, B. Zimmermann, U. Würfel, A. Chafiq, M. Lira-Cantu, T. Swonke, M. Wagner, C. J. Brabec, O. Haillant, E. Voroshazi, T. Aernouts, R. Steim, J. A. Hauch, A. Elschner, M. Pannone, M. Xiao, A. Langzettel, D. Laird, M. T. Lloyd, T. Rath, E. Maier, G. Trimmel, M. Hermenau, T. Menke, K. Leo, R. Rosch, M. Seeland, H. Hoppe, T. J. Nagle, K. B. Burke, C. J. Fell, D.

- Vak, T. B. Singh, S. E. Watkins, Y. Galagan, A. Manor, E. A. Katz, T. Kim, K. Kim, P. M. Sommeling, W. J. H. Verhees, S. C. Veenstra, M. Riede, M. Greyson Christoforo, T. Currier, V. Shrotriya, G. Schwartz and F. C. Krebs, An inter-laboratory stability study of roll-to-roll coated flexible polymer solar modules, *Solar Energy Materials and Solar Cells*, 95, 1398–1416 (2011)
20. J. U. Lee, J. W. Jung, J. W. Jo and W. H. Jo, Degradation and stability of polymer-based solar cells, *J. Mater. Chem.*, 22, 24265-24283 (2012)
21. W. J. Potscavage, S. Yoo, B. Domercq, and B. Kippelen, Encapsulation of pentacene/C₆₀ organic solar cells with Al₂O₃ deposited by atomic layer deposition, *Appl. Phys. Lett.* 90, 253511-253511 (2007)
22. Y. Kanai, T. Matsushima, and H. Murata, Improvement of stability for organic solar cells by using molybdenum trioxide buffer layer, *Thin Solid Films* 518, 537-540 (2009)
23. S. O. Jeon and J. Y. Lee, Improved high temperature stability of organic solar cells using a phosphine oxide type cathode modification layer, *Solar Energy Materials and Solar Cells* 95, 1102-1106 (2011)
24. Y. Wang, L. Yang, C. Yao, W. Qin, S. Yin, and F. Zhang, Enhanced performance and stability in polymer photovoltaic cells using lithium benzoate as cathode interfacial layer, *Solar Energy Materials and Solar Cells* 95, 1243-1247 (2011)
25. R. R. Søndergaard, T. Makris, P. Lianos, A. Manor, E. A. Katz, W. Gong, S. M. Tuladhar, J. Nelson, R. Tuomi, P. Sommeling, S. C. Veenstra, A. Rivaton, A. Dupuis, G. Teran-Escobar, M. Lira-Cantu, S. B. Sapkota, B. Zimmermann, U. Würfel, A. Matzarakism, F. C. Krebs, The use of polyurethane as encapsulating method for polymer solar cells—An inter laboratory

- study on outdoor stability in 8 countries, *Solar Energy Materials and Solar Cells* 99, 292-300 (2012).
26. W. Gaynor, J.-Y. Lee, and P. Peumans, Fully solution-processed inverted polymer solar cells with laminated nanowire electrodes, *ACS Nano* 4, 30-34 (2009)
27. Z. Liang and Q. Wang, in *Handbook of Organic Electronics and Photonics*, edited by H. S. Nalwa, American Scientific Publishers, Los Angeles, CA (2008), volume 1, p. 177-223
28. S. -S. Sun, in *Handbook of Organic Electronics and Photonics*, edited by H. S. Nalwa, American Scientific Publishers, Los Angeles, CA (2008), volume 3, p. 314-350
29. R. Gomez and J. L. Segura, in *Handbook of Organic Electronics and Photonics*, edited by H. S. Nalwa, American Scientific Publishers, Los Angeles, CA (2008), volume 3, p. 35-399
30. M. Girtan and M. Rusu, Role of ITO and PEDOT: PSS in stability/degradation of polymer: fullerene bulk heterojunctions solar cells, *Solar Energy Materials and Solar Cells* 94, 446-450 (2010).
31. P. W. Sutter, J. I. Flege, and E. A. Sutter, Large-scale pattern growth of graphene films for stretchable transparent electrodes, *Nature Mater.* 7, 406–411 (2008),
32. G. Eda, G. Fanchini, and M. Chhowalla, Large-area ultrathin films of reduced graphene oxide as a transparent and flexible electronic material, *Nature Nanotechnol.* 3, 270–274 (2008),
33. K. S. Kim, Y. Zhao, H. Jang, S. Y. Lee, J. M. Kim, K. S. Kim, J.-H. Ahn, P. Kim, J.-Y. Choi, and B. H. Hong, Large-scale pattern growth of graphene films for stretchable transparent electrodes, *Nature* 457, 706-710 (2009).
34. J. C. Meyer, A. K. Geim, M. I. Katsnelson, K. S. Novoselov, T. J. Booth and S. Roth, The structure of suspended graphene sheets, *Nature* 446, 60-63 (2007).

35. D. Li, M. B. Müller, S. Gilje, R. B. Kaner and G. G. Wallace, Processable aqueous dispersions of graphene nanosheets, *Nature Nanotechnol.*, 3, 101-105 (2008)
36. Y. Xu, H. Bai, G. Lu, C. Li, and G. Shi, Flexible Graphene Films via the Filtration of Water-Soluble Noncovalent Functionalized Graphene Sheets, *J. Am. Chem. Soc.* 130, 5856–5857 (2008)
37. I. W. Frank and D. M. Tanenbaum, A. M. van der Zande and P. L. McEuen, Mechanical properties of suspended graphene sheets, *J. Vac. Sci. Technol. B* 25,, 2558-25561 (2007)
38. X. Zhou and Z. Liu, A scalable, solution-phase processing route to graphene oxide and graphene ultralarge sheets, *Chem. Commun.*, 46, 2611-2613 (2010).
39. Y.-W. Son, M. L. Cohen, and S. G. Louie, Half-metallic graphene nanoribbons, *Nature* 444, 347-349 (2006).
40. M. Y. Han, B. Ozyilmaz, Y. B. Zhang, and P. Kim, Energy band-gap engineering of graphene nanoribbons, *Phys. Rev. Lett.* 98, 206805 (2007).
41. X. Li, X. Wang, L. Zhang, S. Lee, H. Dai, Chemically Derived, Ultrasoft Graphene Nanoribbon Semiconductors, *Science* 319, 1229-1232 (2008)
42. H. Chen, M. B. Muller, K. J. Gilmore, G. G. Wallace, and D. Li, Mechanically Strong, Electrically Conductive, and Biocompatible Graphene Paper, *Adv. Mater.*, 20, 3557–3561 (2008).
43. F. Yavari, Z. Chen, A. V. Thomas, W. Ren, H.-M. Cheng, N. Koratkar, High Sensitivity Gas Detection Using a Macroscopic Three-Dimensional Graphene Foam Network, *Scientific Reports*, 1, (2011), Article number 166; doi:10.1038/srep00166

44. Z. Chen, C. Xu, C. Ma, W. Ren and H.-M. Cheng, Lightweight and Flexible Graphene Foam Composites for High-Performance Electromagnetic Interference Shielding, *Adv. Mater.* 25, 1296–1300 (2013).
45. M. D. Stoller, S. Park, Y. Zhu, J. An, and R. S. Ruoff, Graphene-based ultracapacitors, *Nano Lett.* 8, 3498-3502 (2008)
46. E. Kymakis, K. Savva, M. M. Stylianakis, C. Fotakis, and E. Stratakis, Flexible Organic Photovoltaic Cells with In Situ Nonthermal Photoreduction of Spin-Coated Graphene Oxide Electrodes, *Adv. Func. Mater.* 23, 2742-2749 (2013)
47. D. Konios, C. Petridis, G. Kakavelakis, M. Sygletou, K. Savva, E. Stratakis, and E. Kymakis, Reduced Graphene Oxide Micromesh Electrodes for Large Area, Flexible, Organic Photovoltaic Devices, *Adv. Func. Mater.* 25, 2213-2221 (2015)
48. E. Kymakis, N. Balis, D. Konios, and E. Stratakis, Ternary organic solar cells with reduced graphene oxide-Sb₂S₃ hybrid nanosheets as the cascade material, *ChemNanoMat* (2015), DOI: 10.1002/cnma.201500044
49. F. Bonaccorso, L. Colombo, G. Yu, M. Stoller, V. Tozzini, A. C. Ferrari, R. S. Ruoff, and V. Pellegrini, Graphene, related two-dimensional crystals, and hybrid systems for energy conversion and storage, *Science* 347, 1246501 (2015)
50. C.-H. Lu, H.-H. Yang, C.-L. Zhu, X. Chen, and G.-N. Chen, A graphene platform for sensing biomolecules, *Angew. Chem.* 121, 4879-4881 (2009)
51. G. M. Viskadourous, M. M. Stylianakis, E. Kymakis, and E. Stratakis, Enhanced field emission from reduced graphene oxide polymer composites, *ACS Appl. Mater. Interfaces* 6, 388-393 (2013)

52. G. Viskadourous, D. Konios, E. Kymakis, and E. Stratakis, Direct laser writing of flexible graphene field emitters, *Appl. Phys. Lett.* 105, 203104 (2014)
53. S. Bae, H. Kim, Y. Lee, X. Xu, J.-S. Park, Y. Zheng, J. Balakrishnan, T. Lei, H. R. Kim, Y. I. Song, Y. J. Kim, K. S. Kim, B. Ozyilmaz, J.-H. Ahn, B. H. Hong and S. Iijima, Roll-to-roll production of 30-inch graphene films for transparent electrodes, *Nature Nanotechnol.* 5, 574-578 (2010)
54. A. Lerf, H. Y. He, and M. Forster, J. Klinowski, Structure of graphite oxide revisited. *J. Phys. Chem. B* 102, 4477– 4482 (1998);
55. H. He, J. Klinowski, M. Forster and A. Lerf, A new structural model for graphite oxide, *Chem. Phys. Lett.*, 287, 53–56 (1998)
56. W. Gao, L. B. Alemany, L. Ci, and P. M. Ajayan, New insights into the structure and reduction of graphite oxide, *Nature Chem.*, 1, 403-408 (2009)
57. (a) K. S. Novoselov, A. K. Geim, S. V. Morozov, D. Jiang, Y. Zhang, S. V. Dubonos, I. V. Grigorieva, and A. A. Firsov, Electric Field Effect in Atomically Thin Carbon Films, *Science*, 306, 666-669 (2004); (b) A. K. Geim and K. S. Novoselov, The rise of graphene. *Nature Mater.* 6, 183–191 (2007); (c) R. R. Nair, P. Blake, A. N. Grigorenko, K. S. Novoselov, T. J. Booth, T. Stauber, N. M. R. Peres, and A. K. Geim, Fine structure constant defines visual transparency of graphene, *Science* 320, 1308-1308 (2008)
58. Z. Wang, D. Xu, Y. Huang, Z. Wu, L. Wang and X. Zhang, Facile, mild and fast thermal-decomposition reduction of graphene oxide in air and its application in high-performance lithium batteries, *Chem. Commun.*, 48, 976-978 (2012)

59. A. Mathkar, D. Tozier, P. Cox, P. Ong, C. Galande, K. Balakrishnan, A. L. M. Reddy and P. M. Ajayan, Controlled, Stepwise Reduction and Band Gap Manipulation of Graphene Oxide. *J. Phys. Chem. Lett.*, *3*, 986-991 (2012)
60. S. Park, J. An, J. R. Potts, A. Velamakanni, S. Murali, and R. S. Ruoff, Hydrazine-reduction of graphite-and graphene oxide, *Carbon* *49*, 3019-3023 (2011)
61. M. Acik, G. Lee, C. Mattevi, A. Pirkle, R. M. Wallace, M. Chhowalla, K. Cho and Y. Chabal, The Role of Oxygen during Thermal Reduction of Graphene Oxide Studied by Infrared Absorption Spectroscopy. *J. Phys. Chem. C.*, *115*, 19761-19781 (2011).
62. L. Zhang, J. Liang, Y. Huang, Y. Ma, Y. Wang, Y. Chen, Size-controlled synthesis of graphene oxide sheets on a large scale using chemical exfoliation, *Carbon*, *47*, 3365-3380 (2009)
63. J. Shen, Y. Hu, C. Li, C. Qin, M. Shi, and M. Ye, Layer-by-Layer Self-Assembly of Graphene Nanoplatelets, *Langmuir* *25*, 6122–6128 (2009)
64. L. Sun and B. Fugetsu, Mass production of graphene oxide from expanded graphite, *Mater. Lett.*, *109*, 207-210 (2013)
65. D. Konios, M. M. Stylianakis, E. Stratakis, and E. Kymakis, Dispersion behaviour of graphene oxide and reduced graphene oxide, *J. Colloid Interface Sci.* *430*, 108-112 (2014)
66. A. Bianco, H.-M. Cheng, T. Enoki, Y. Gogotsi, R. H. Hurt, K. Koratkar, T. Kyotanic, M. Monthieux, C. R. Park, J. M. D. Tacon, J. Zhang, All in the graphene family-A recommended nomenclature for two-dimensional carbon materials, *Carbon*, *65*, 1–6 (2013)
67. P. Wick, A. E. Louw-Gaume, M. Kucki, H. F. Krug, K. Kostarelos, B. Fadeel, K. A. Dawson, A. Salvati, E. Vazquez, L. Ballerini, M. Tretiach, F. Benfenati, E. Flahaut, L.

- Gauthier, M. Prato, and A. Bianco, Classification Framework for Graphene-Based Materials, *Angew. Chem. Int. Ed.* 53, 7714-7718 (2014)
68. F. Bonaccorso, A. Lombardo, T. Hasan, Z. Sun, L. Colombo, and A. C. Ferrari, Production and processing of graphene and 2d crystals, *Mater. Today* 15, 564-589 (2012)
69. X. Huang, Z. Yin, S. Wu, X. Qi, Q. He, Q. Zhang, Q. Yan, F. Boey, and H. Zhang, Graphene-based materials: synthesis, characterization, properties, and applications, *Small* 7, 1876-1902 (2011)
70. S. Park and R. S. Ruoff, Chemical methods for the production of graphenes, *Nature Nanotechnol.* 4, 217-224 (2009)
71. D. R. Dreyer, S. Park, C. W. Bielawski, and R. S. Ruoff, The chemistry of graphene oxide, *Chem. Soc. Rev.* 39, 228-240 (2010)
72. D. R. Dreyer, A. D. Todd, and C. W. Bielawski, Harnessing the chemistry of graphene oxide, *Chem. Soc. Rev.* 43, 5288-5301 (2014)
73. C. K. Chua, and M. Pumera, Chemical reduction of graphene oxide: a synthetic chemistry viewpoint, *Chem. Soc. Rev.* 43, 291-312 (2014)
74. O. C. Compton and S. T. Nguyen, Graphene Oxide, Highly Reduced Graphene Oxide, and Graphene: Versatile Building Blocks for Carbon-Based Materials, *Small* 6, 711-723 (2010)
75. V. Georgakilas, M. Otyepka, A. B. Bourlinos, V. Chandra, N. Kim, K. C. Kemp, P. Hobza, R. Zboril, and K. S. Kim, Functionalization of graphene: covalent and non-covalent approaches, derivatives and applications, *Chem. Rev.*, 112, 6156-6214 (2012)
76. Y. Zhu, S. Murali, W. Cai, X. Li, J. W. Suk, J. R. Potts, and R. S. Ruoff, Graphene and graphene oxide: synthesis, properties, and applications, *Adv. Mater.* 22, 3906-3924 (2010)

77. K. R. Paton, E. Varrla, C. Backes, R. J. Smith, U. Khan, A. O'Neill, C. Boland, M. Lotya, O. M. Istrate, P. King, T. Higgins, S. Barwich, P. May, P. Puczkarski, I. Ahmed, M. Moebius, H. Pettersson, E. Long, J. Coelho, S. E. O'Brien, E. K. McGuire, B. M. Sanchez, G. S. Duesberg, N. McEvoy, T. J. Pennycook, C. Downing, A. Crossley, V. Nicolosi and J. N. Coleman, Scalable production of large quantities of defect-free few-layer graphene by shear exfoliation in liquids *Nature Mater.* 13, 624-630 (2014)
78. H. P. Cong, J.-F. Chen, and S.-H. Yu, Graphene-based macroscopic assemblies and architectures: an emerging material system, *Chem. Soc. Rev.* 43, 7295-7325 (2014)
79. A. Ambrosi, C. K. Chua, A. Bonanni, and M. Pumera, Electrochemistry of graphene and related materials, *Chem. Rev.* 114, 7150-7188 (2014)
80. R. Raccichini, A. Varzi, S. Passerini, and B. Scrosati, The role of graphene for electrochemical energy storage, *Nature Mater.* 14, 271-279 (2015)
81. J. Zhu, D. Yang, Z. Yin, Q. Yan, and H. Zhang, Graphene and Graphene-Based Materials for Energy Storage Applications, *Small* 10, 3480-3498 (2014)
82. C. Xie, X. Z. Zhang, Y. M. Wu, X. J. Zhang, X. W. Zhang, Y. Wang, W. J. Zhang, P. Gao, Y. Y. Han, and J. S. Jie, Surface passivation and band engineering: a way toward high efficiency graphene–planar Si solar cells, *J. Mater. Chem. A* 1, 8567-8574 (2013)
83. Y. Tsuboi, F. Wang, D. Kozawa, K. Funahashi, S. Mouri, Y. Miyauchi, T. Takenobu, and K. Matsuda, Enhanced Photovoltaic Performances of Graphene/Si Solar Cells by Insertion of an MoS₂ Thin Film, *arXiv preprint arXiv:1503.05380* (2015).
84. Q. Xu, T. Song, W. Cui, Y. Liu, W. Xu, S.-T. Lee, and B. Sun, Solution-Processed Highly-Conductive PEDOT: PSS/AgNWs/GO Transparent Film for Efficient Organic-Si Hybrid Solar Cells, *ACS Appl. Mater. Interfaces*, 7, 3272–3279 (2015)

85. X. Li, S. Zhang, P. Wang, H. Zhong, Z. Wu, H. Chen, C. Liu, and S. Lin, High performance solar cells based on graphene/GaAs heterostructures, arXiv:1409.3500v2 (2014)
86. Y. Song, X. Li, C. Mackin, X. Zhang, W. Fang, T. Palacios, H. Zhu, and J. Kong, Role of Interfacial Oxide in High-Efficiency Graphene–Silicon Schottky Barrier Solar Cells, *Nano Lett.*, 15, 2104–2110 (2015)
87. A. R. bin M. Yusoff, D. Kim, F. K. Schneider, W. Jose da Silva, and J. Jang, Au-doped single layer graphene nanoribbons for a record-high efficiency ITO-free tandem polymer solar cell, *Energy Environ. Sci.* 8, 1523-1537 (2015)
88. J. T. W. Wang, J. M. Ball, E. M. Barea, A. Abate, J. A. Alexander-Webber, J. Huang, M. Saliba, I. Mora-Sero, J. Bisquert, H. J. Snaith, and R. J. Nicholas, Low-Temperature Processed Electron Collection Layers of Graphene/TiO₂ Nanocomposites in Thin Film Perovskite Solar Cells, *Nano Lett.*, 14, 724–730 (2014)
89. L. B. Groenendaal, F. Jonas, D. Freitag, H. Pielartzik, J. R. Reynolds, Poly(3,4-ethylenedioxythiophene) and Its Derivatives: Past, Present, and Future, *Adv. Mater.* 12, 481-494 (2000)
90. S. Kirchmeyer, K. Reuter, Scientific importance, properties and growing applications of poly(3,4-ethylenedioxythiophene), *J. Mater. Chem.* 15, 2077-2088 (2005)
91. J. Huang, P. F. Miller, J. C. De Mello, A. J. De Mello, and D. D. C. Bradley, Influence of thermal treatment on the conductivity and morphology of PEDOT/PSS films, *Synth. Met.*, 139, 569-572 (2003)
92. J. Huang, P. F. Miller, J.S. Wilson, A. J. de Mello, J. C. de Mello, D. D. C. Bradley, Investigation of the Effects of Doping and Post-Deposition Treatments on the Conductivity,

- Morphology, and Work Function of Poly(3,4-ethylenedioxythiophene)/Poly(styrene sulfonate) Films, *Adv. Funct. Mater.* 15, 290-296 (2005)
93. A. M. Nardes, M. Kemerink, M. M. De Kok, E. Vinken, K. Maturova, and R. A. J. Janssen, Conductivity, work function, and environmental stability of PEDOT: PSS thin films treated with sorbitol, *Organic Electronics* 9, 727-734 (2008)
94. S. Ashizawa, R. Horikawa, H. Okuzaki, Effects of solvent on carrier transport in poly(3,4-ethylenedioxythiophene)/poly(4-styrenesulfonate), *Synth. Met.* 153, 5-8 (2005)
95. E. Kymakis, G. Klapsis, E. Koudoumas, E. Stratakis, N. Kornilios, N. Vidakis, and Y. Franghiadakis, Carbon nanotube/PEDOT: PSS electrodes for organic photovoltaics, *Eur. Phys. J. Appl. Phys.* 36, 257-259 (2006)
96. L. S. C. Pingree, B. A. MacLeod, D. S. Ginger, The Changing Face of PEDOT:PSS Films: Substrate, Bias, and Processing Effects on Vertical Charge Transport, *J. Phys. Chem. C*, 112, 7922-7927 (2008)
97. A. M. Nardes, M. Kemerink, R. A. J. Janssen, J. A. M. Bastiaansen, N. M. M. Kiggen, B. M. W. Langeveld, A. J. J. M van Breemen, and M. M. de Kok, Microscopic understanding of the anisotropic conductivity of PEDOT: PSS thin films, *Adv. Mater.* 19, 1196-1200 (2007)
98. Q. Wei, M. Mukaida, Y. Naitoh and T. Ishida, Morphological Change and Mobility Enhancement in PEDOT:PSS by Adding Co-solvents, *Adv. Mater.*, 25, 2831-2836 (2013)
99. Y. Gao, H.-L. Yip, K.-S. Chen, K. M. O'Malley, O. Acton, Y. Sun, G. Ting, H. Chen, and A. K.-Y. Jen, Surface doping of conjugated polymers by graphene oxide and its application for organic electronic devices, *Adv. Mater.* 23, 1903-1908 (2011)

100. K. Kawano, R. Pacios, D. Poplavskyy, J. Nelson, D. D. C. Bradley, and J. R. Durrant, Degradation of organic solar cells due to air exposure, *Solar Energy Materials and Solar Cells* 90, 3520-3530 (2006)
101. K. Norrman, S. A. Gevorgyan, and F. C. Krebs, Water-induced degradation of polymer solar cells studied by H₂¹⁸O labeling, *ACS Appl. Mater. Interfaces* 1, 102-112 (2008)
102. E. Voroshazi, B. Verreet, A. Buri, R. Müller, D. Di Nuzzo, and P. Heremans, Influence of cathode oxidation via the hole extraction layer in polymer: fullerene solar cells, *Organic Electronics* 12, 736-744 (2011)
103. H. Hoppe and N. S. Sariciftci. Organic solar cells: An overview. *J. Mater. Res*, 19, 1924-1945 (2004);
104. G. Dennler, M. C. Scharber, and C. J. Brabec, Polymer-Fullerene Bulk heterojunction Solar Cells, *Adv. Mater.* 21, 1323–1338 (2009)
105. N. S. Sariciftci and A. J. Heeger, in *Handbook of Organic Conductive Molecules and Polymers*, edited by H. S. Nalwa, John Wiley & Sons Ltd., Chichester, U.K. (1997), volume 1, p. 413-455
106. P. W. M. Blom, V. D. Mihailetschi, L. J. A. Koster, and D. E. Markov, Device physics of polymer: fullerene bulk heterojunction solar cells, *Adv. Mater.* 19, 12 1551-1566 (2007)
107. E. Singh and H. S. Nalwa, Graphene-based bulk-heterojunction solar cells: A Review, *J. Nanosci. Nanotechnol.*, 15, 6237-6278 (2015)
108. E. Singh and H. S. Nalwa, Graphene-based dye-sensitized solar cells: A Review, *Sci. Adv. Mater.*, 7 (10), (2015) doi:10.1166/sam.2015.2438

109. X. Liu, H. Kim and L. J. Guo, Optimization of thermally reduced graphene oxide for an efficient hole transport layer in polymer solar cells, *Organic Electronics*, 14, 591-598 (2013)
110. I. P. Murray, S. J. Lou, L. J. Cote, S. Loser, C. J. Kadleck, T. Xu, J. M. Szarko, B. S. Rolczynski, J. E. Johns, J. Huang, L. Yu, L. X. Chen, T. J. Marks, and M. C. Hersam, Graphene oxide interlayers for robust, high-efficiency organic photovoltaics, *J. Phys. Chem. Lett.* 2, 3006-3012 (2011)
111. K. C. Kwon, W. J. Dong, G. H. Jung, J. Ham, J.-L. Lee, and S. Y. Kim, Extension of stability in organic photovoltaic cells using UV/ozone-treated graphene sheets, *Solar Energy Materials and Solar Cells* 109, 148-154 (2013)
112. H. P. Kim, A. R. bin Mohd Yusoff, M. S. Ryu, and J. Jang, Stable photovoltaic cells based on graphene oxide/indium zinc oxide bilayer anode buffer, *Organic Electronics* 13, 3195-3202 (2012)
113. Q. -D. Yang, T.-W. Ng, M.-F. Lo, N.-B. Wong, and C.-S. Lee, Enhanced storage/operation stability of small molecule organic photovoltaics using graphene oxide interfacial layer, *Organic Electronics* 13, 3220-3225 (2012)
114. D. Lee, H. Lee, Y. Ahn, Y. Jeong, D.-Y. Lee, and Y. Lee. Highly stable and flexible silver nanowire-graphene hybrid transparent conducting electrodes for emerging optoelectronic devices, *Nanoscale* 5, 7750-7755 (2013)
115. Y. Ahn, Y. Jeong, and Y. Lee, Improved thermal oxidation stability of solution-processable silver nanowire transparent electrode by reduced graphene oxide, *ACS Appl. Mater. Interfaces* 4, 6410-6414 (2012)

116. L. Yang, X. Yu, W. Hu, X. Wu, Y. Zhao, and D. Yang, An 8.68% Efficiency Chemically-Doped-Free Graphene-Silicon Solar Cell Using Silver Nanowires Network Buried Contacts, *ACS Appl. Mater. Interfaces* 7, 4135-4141 (2015).
117. J.-S. Yeo, R. Kang, S. Lee, Y.-J. Jeon, N. S. Myoung, C.-L. Lee, D.-Y. Kim, J.-M. Yun, Y.-H. Seo, S.-S. Kim, S.-I. Na, Highly efficient and stable planar perovskite solar cells with reduced graphene oxide nanosheets as electrode interlayer, *Nano Energy*, 12, 96–104 (2015)
118. J. M. Yun, J.-S. Yeo, J. Kim, H.-G. Jeong, D.-Y. Kim, Y.-J. Noh, S.-S. Kim, B.-C. Ku, and S.-I. Na, Solution-Processable Reduced Graphene Oxide as a Novel Alternative to PEDOT:PSS Hole-transport layers for Highly Efficient and Stable Polymer Solar Cells, *Adv. Mater.* 23, 4923-4928 (2011)
119. Z. Liu, Q. Liu, Y. Huang, Y. Ma, S. Yin, X. Zhang, W. Sun, and Y. Chen, Organic Photovoltaic Devices Based on a Novel Acceptor Material: Graphene, *Adv. Mater.* 20, 3924-3930 (2008)
120. T. Cui, R. Lv, Z.-H. Huang, S. Chen, Z. Zhang, X. Gan, Y. Jia, X. Li, K. Wang, D. Wu and F. Kang, Enhanced efficiency of graphene/silicon heterojunction solar cells by molecular doping, *J. Mater. Chem. A*, 1, 5736-5740 (2013)
121. C. Xie, X. Zhang, K. Ruan, Z. Shao, S. S. Dhaliwal, L. Wang, Q. Zhang, X. Zhang, J. Jie, High-Efficiency, Air Stable Graphene/Si Micro-Hole Array Schottky Junction Solar Cells. *J. Mater. Chem. A* 1, 15348-15354 (2013)
122. X. Z. Zhang, C. Xie, J. S. Jie, X. W. Zhang, Y. M. Wu and W. J. Zhang, High-efficiency graphene/Si nanoarray Schottky junction solar cells *via* surface modification and graphene doping, *J. Mater. Chem. A*, 1, 6593-6601 (2013)

123. E. Shi, H. Li, L. Yang, L. Zhang, Z. Li, P. Li, Y. Shang, S. Wu, X. Li, J. Wei, K. Wang, H. Zhu, D. Wu, Y. Fang, and A. Cao, Colloidal antireflection coating improves graphene–silicon solar cells, *Nano Lett.* 13, 1776-1781 (2013)
124. V. V. Brus, M. A. Gluba, X. Zhang, K. Hinrichs, J. Rappich, and N. H. Nickel, Stability of graphene–silicon heterostructure solar cells, *Phys. Status Solidi A*, 211, 843–847 (2014)
125. L. Lancellotti, E. Bobeico, A. Capasso, M. Della Noce, T. Dikonimos, N. Lisi, and P. DelliVeneri, Effects of HNO₃ molecular doping in graphene/Si Schottky barrier solar cells. In Proceedings of Conference on Photonics Technologies, 2014 Fotonica AEIT Italian, IEEE, Naples, Italy. 12-14 May 2014, p.1-3.
<http://dx.doi.org/10.1109/Fotonica.2014.6843898>
126. X. Li, H. Zhu, K. Wang, J. Wei, G. Fan, X. Li, and D. Wu, Chemical Doping and Enhanced Solar Energy Conversion of Graphene/Silicon Junctions, *arxiv.org/pdf/1012.5730* (2010)
127. H. B. Yang, Y. Q. Dong, X. Wang, S. Y. Khoo, and B. Liu, Cesium Carbonate Functionalized Graphene Quantum Dots as Stable Electron-Selective Layer for Improvement of Inverted Polymer Solar Cells, *ACS Appl. Mater. Interfaces*, 6, 1092–1099 (2014)
128. J. Liu, G.-H. Kim, Y. Xue, J. Y. Kim, J. -B. Baek, M. Durstock, and L. Dai, Graphene Oxide Nanoribbon as Hole Extraction Layer to Enhance Efficiency and Stability of Polymer Solar Cells, *Adv. Mater.*, 26, 786–790, (2014)
129. D. H. Wang, J. K. Kim, J. H. Seo, I. Park, B. H. Hong, J. H. Park, and A. J. Heeger, Transferable Graphene Oxide by Stamping Nanotechnology: Electron-Transport Layer for Efficient Bulk-Heterojunction Solar Cells, *Angew. Chem. Int. Ed.* 52, 2874-2880 (2013)

130. Y.-J. Jeon, J.-M. Yun, D.-Y. Kim, S.-I. Na, and S.-S. Kim, High-performance polymer solar cells with moderately reduced graphene oxide as an efficient hole transporting layer, *Solar Energy Materials and Solar Cells* 105, 96-102 (2012)
131. L. Chen, D. Du, K. Sun, J. Hou, and J. Ouyang, Improved Efficiency and Stability of Polymer Solar Cells Utilizing Two-Dimensional Reduced Graphene Oxide: Graphene Oxide Nanocomposites as Hole-Collection Material, *ACS Appl. Mater. Interfaces*, 6, 22334–22342 (2014)
132. H. P. Kim, Abd. R. M. Yusoff and J. Jang, High performance and stability of chemically modified graphene oxide organic solar cells, in *Materials and processes for energy: communicating current research and technological developments*, Edited by A. Mendez-Vilas, Formatex Research Center, Badajoz, Spain (2013). pp. 68-74
133. C. Li, Z. Li, H. Zhu, K. Wang, J. Wei, X. Li, P. Sun, H. Zhang and D. Wu, Graphene Nano-“patches” on a Carbon Nanotube Network for Highly Transparent/Conductive Thin Film Applications, *J. Phys. Chem. C*, 114, 14008–14012 (2010)
134. A. R. bin Mohd Yusoff, H. P. Kim, and J. Jang, Inverted organic solar cells with TiO_x cathode and graphene oxide anode buffer layers, *Solar Energy Materials and Solar Cells* 109, 63-69 (2013)
135. H. P. Kim, A. R. bin Mohd Yusoff, and J. Jang, Organic solar cells using a reduced graphene oxide anode buffer layer, *Solar Energy Materials and Solar Cells*, 110, 87–93 (2013)
136. E. Stratakis, M. M. Stylianakis, E. Koudoumas, and E. Kymakis, Plasmonic organic photovoltaic devices with graphene based buffer layers for stability and efficiency enhancement, *Nanoscale* 5, 4144-4150 (2013)

137. P. Li, C. Chen, J. Zhang, S. Li, B. Sun, and Q. Bao, Graphene-based transparent electrodes for hybrid solar cells, *Frontiers in Materials*, volume 1, article 26, 1-7 (2014)
doi:10.3389/fmats.2014.00026
138. P. Gao, K. Ding, Y. Wang, K. Ruan, S. Diao, Q. Zhang, B. Sun, and J. Jie, Crystalline Si/Graphene Quantum Dots Heterojunction Solar Cells, *J. Phys. Chem. C* 118, 5164–5171 (2014)
139. G. Williams, Q. Wang, and H. Aziz, The photo-stability of polymer solar cells: Contact photo-degradation and the benefits of interfacial layers, *Adv. Func. Mater.*, 23, 2239-2247 (2013)
140. M. Giannouli, V. M. Drakonakis, A. Savva, P. Eleftheriou, G. Florides, and S. A. Choulis, Methods for Improving the Lifetime Performance of Organic Photovoltaics with Low-Costing Encapsulation, *ChemPhysChem* 16, 1134-1154 (2015)
141. L. La Notte, G. Polino, P. Verzola, L. Salamandra, F. Brunetti, T. M. Brown, A. Di Carlo, and A. Reale, Influence of encapsulation materials on the optical properties and conversion efficiency of heat-sealed flexible polymer solar cells, *Surf. Coat. Technol.*, 255, 69-73 (2014)
142. S. B. Sapkota, A. Spies, B. Zimmermann, I. Dürr, and U. Würfel, Promising long-term stability of encapsulated ITO-free bulk-heterojunction organic solar cells under different aging conditions, *Solar Energy Materials and Solar Cells* 130, 144-150 (2014)
143. M. S. Ryu, H. J. Cha, and J. Jang, Improvement of operation lifetime for conjugated polymer: fullerene organic solar cells by introducing a UV absorbing film, *Solar Energy Materials and Solar Cells* 94, 152-156 (2010).

144. J. W. Rumer, R. S. Ashraf, N. D. Eisenmenger, Z. Huang, I. Meager, C. B. Nielsen, B. C. Schroeder, M. L. Chabinyc, and I. McCulloch, Dual Function Additives: A Small Molecule Crosslinker for Enhanced Efficiency and Stability in Organic Solar Cells, *Adv. Energy Mater.* 2015, 1401426 (2015)
145. T. Tromholt, M. V. Madsen, J. E. Carlé, M. Helgesen, and F. C. Krebs, Photochemical stability of conjugated polymers, electron acceptors and blends for polymer solar cells resolved in terms of film thickness and absorbance, *J. Mater. Chem.* 22, 7592-7601 (2012)
146. M. Hermenau, S. Schubert, H. Klumbies, J. Fahlteich, L. Müller-Meskamp, K. Leo, and M. Riede, The effect of barrier performance on the lifetime of small-molecule organic solar cells, *Solar Energy Materials and Solar Cells* 97, 102-108 (2012)
147. S. A. Gevorgyan, M. V. Madsen, H. F. Dam, M. Jørgensen, C. J. Fell, K. F. Anderson, B. C. Duck, A. Mescheloff, E. A. Katz, A. Elschner, R. Roesch, H. Hoppe, M. Hermenau, M. Riede, F. C. Krebs, Interlaboratory outdoor stability studies of flexible roll-to-roll coated organic photovoltaic modules: Stability over 10,000 h, *Solar Energy Materials & Solar Cells*, 116, 187–196 (2013)
148. R. Po, C. Carbonera, A. Bernardi, and N. Camaioni, The role of buffer layers in polymer solar cells, *Energy Environ. Sci.*, 4, 285–310 (2010)
149. K. Kawano and C. Adachi, Reduced initial degradation of bulk heterojunction organic solar cells by incorporation of stacked fullerene and lithium fluoride interlayers, *Appl. Phys. Lett.*, 96, 053307 (2010)
150. V. Shrotriya, G. Li, Y. Yao, C. W. Chu, and Y. Yang, Transition metal oxides as the buffer layer for polymer photovoltaic cells, *Appl. Phys. Lett.*, 88, 073508 (2006)

151. A. Roy, S. H. Park, S. Cowan, M. H. Tong, S. Cho, K. Lee, and A. J. Heeger, Titanium suboxide as an optical spacer in polymer solar cells, *Appl. Phys. Lett.*, 95, 013302 (2009)
152. J. Li, S. Kim, S. Edington, J. Nedy, S. Cho, K. Lee, A. J. Heeger, M. C. Gupta, and J. T. Yates, A study of stabilization of P3HT/PCBM organic solar cells by photochemical active TiO_x layer, *Solar Energy Materials and Solar Cells* 95, 1123-1130 (2011)
153. G. Teran-Escobar, D. M. Tanenbaum, E. Voroshazi, M. Hermenau, K. Norrman, M. T. Lloyd, Y. Galagan, B. Zimmermann, M. Hoesel, H. F. Dam, M. Jorgensen, S. Gevorgyan, S. Kudret, W. Maes, L. Lutsen, D. Vanderzande, U. Würfel, R. Andriessen, R. Roesch, H. Hoppe, A. Rivaton, G. Y. Uzunoglu, D. Germack, B. Andreasen, M. V. Madsen, E. Bundgaard, F. C. Krebs, and M. Lira-Cantu, On the stability of a variety of organic photovoltaic devices by IPCE and in situ IPCE analyses situ IPCE analyses and absorbance, *Phys. Chem. Chem. Phys.*, 14, 11824.11845 (2012)
154. M. O. Reese, S. A. Gevorgyan, M. Jorgensen, E. Bundgaard, S. R. Kurtz, D. S. Ginley, D. C. Olson, M. T. Lloyd, P. Morvillo, E. A. Katz, A. Elschner, O. Haillant, T. R. Currier, V. Shrotriya, M. Hermenau, M. Riede, K. R. Kirov, G. Trimmel, T. Rath, O. Inganas, F. Zhang, M. Andersson, K. Tvingstedt, M. Lira-Cantu, D. Laird, C. McGuinness, S. Gowrisanker, M. Pannone, M. Xiao, J. Hauch, R. Steim, D. M. DeLongchamp, R. Roesch, H. Hoppe, N. Espinosa, A. Urbina, G. Yaman-Uzunoglu, J.-B. Bonekamp, A. J. J. M. van Breemen, C. Girotto, E. Voroshazi and F. C. Krebs, Consensus stability testing protocols for organic photovoltaic materials and devices, *Solar Energy Materials and Solar Cells*, 95, 1253–1267 (2011)
155. J. Kesters, P. Verstappen, J. Raymakers, W. Vanormelingen, J. Drijkoningen, J. D'Haen, J. Manca, L. Lutsen, D. Vanderzande, and W. Maes, Enhanced Organic Solar Cell Stability

- by Polymer (PCPDTBT) Side Chain Functionalization, *Chem. Mater.* 27, 1332-1341 (2015)
156. C. H. Peters, I. T. Sachs-Quintana, J. P. Kastrop, S. Beaupré, M. Leclerc, and M. D. McGehee, High efficiency polymer solar cells with long operating lifetimes, *Adv. Energy Mater.* 1, 491-494 (2011)
157. J. Kong, S. Song, M. Yoo, G. Y. Lee, O. Kwon, J. K. Park, H. Back, G. Kim, S. H. Lee, H. Suh, and K. Lee, Long-term stable polymer solar cells with significantly reduced burn-in loss, *Nature Commun.*, 5, Article number 5688, (2014).
158. A. Seemann, H-J. Egelhaaf, C. J. Brabec, and J. A. Hauch, Influence of oxygen on semi-transparent organic solar cells with gas permeable electrodes, *Organic Electronics* 10, 1424-1428 (2009)
159. M. Hermenau, M. Riede, K. Leo, S. A. Gevorgyan, F. C. Krebs, and K. Norrman, Water and oxygen induced degradation of small molecule organic solar cells, *Solar Energy Materials and Solar Cells* 95, 1268-1277 (2011)
160. E. Voroshazi, B. Verreet, A. Buri, R. Müller, D. Di Nuzzo, and P. Heremans, Influence of cathode oxidation via the hole extraction layer in polymer: fullerene solar cells, *Organic Electronics* 12, 736-744 (2011)
161. X. Wang, C. X. Zhao, G. Xu, Z.-K. Chen, and F. Zhu, Degradation mechanisms in organic solar cells: Localized moisture encroachment and cathode reaction, *Solar Energy Materials and Solar Cells* 104, 1-6 (2012).
162. B. Zimmermann, U. Würfel, and M. Niggemann, Longterm stability of efficient inverted P3HT: PCBM solar cells, *Solar Energy Materials and Solar Cells* 93, 491-496 (2009)

163. A. Seemann, T. Sauermann, C. Lungenschmied, O. Armbruster, S. Bauer, H-J. Egelhaaf, and J. Hauch, Reversible and irreversible degradation of organic solar cell performance by oxygen, *Solar Energy* 85, 1238-1249 (2011)
164. http://cordis.europa.eu/project/rcn/101561_en.html
165. M. L. Tongay, T. Schumann, K. Berke, B. Gila, B. R. Appleton, and A. F. Hebard, Graphene/GaN Schottky diodes: Stability at Elevated Temperatures, *Appl. Phys. Lett.* 99, 102102 (2011)
166. E. Stratakis, K. Savva, D. Konios, C. Petridis and E. Kymakis, Improving the efficiency of organic photovoltaics by tuning the work function of graphene oxide hole transporting layers, *Nanoscale*, 6, 6925-6931 (2014)
167. G. Kakavelakis, D. Konios, E. Stratakis, and E. Kymakis, Enhancement of the efficiency and stability of organic photovoltaic devices via the addition of a lithium-neutralized graphene oxide electron-transporting layer, *Chem. Mater.* 26, 5988-5993 (2014)
168. J. S. Bunch, S. S. Verbridge, J. S. Alden, A. M. van der Zande, J. M. Parpia, H. G. Craighead and P. L. McEuen, Impermeable Atomic Membranes from Graphene Sheets, *Nano Lett.*, 8, 2458 (2008)
169. T. Kim, J. H. Kang, S. J. Yang, S. J. Sung, Y. S. Kim and C. R. Park, Facile preparation of reduced graphene oxide based gas barrier films for organic photovoltaic devices, *Energy Environ. Sci.*, 7, 3403-3411 (2014)
170. Y. Ahn, Y. Jeong, D. Lee, and Y. Lee, Copper Nanowire–Graphene Core–Shell Nanostructure for Highly Stable Transparent Conducting Electrodes, *ACS Nano* 9, 3125-3133 (2015)

171. J. -K. Yeo, J. -M. Yun, Y.-S. Jung, D.-Y. Kim, Y.-J. Noh, S.-S. Kim, and S.-I. Na, Sulfonic acid-functionalized, reduced graphene oxide as an advanced interfacial material leading to donor polymer-independent high-performance polymer solar cells, *J. Mater. Chem. A*, 2, 292-298 (2014).
172. N. Kim, G. Xin, S. M. Cho, C. Pang, and H. Chae, Microwave-reduced graphene oxide for efficient and stable hole extraction layers of polymer solar cells, *Current Appl. Phys.* 15, 953–957 (2015).
173. S. B. Sapkota, A. Spies, B. Zimmermann, I. Dürr, and U. Würfel, Promising long-term stability of encapsulated ITO-free bulk-heterojunction organic solar cells under different aging conditions, *Solar Energy Materials and Solar Cells* 130, 144-150 (2014)
174. S. Singh, and H. S. Nalwa, Nanotechnology and health safety–toxicity and risk assessments of nanostructured materials on human health, *J. Nanosci. Nanotechnol.* 7, 3048-3070 (2007)
175. Y. L. Zhao and H. S. Nalwa, (eds.), *Nanotoxicology-Interactions of Nanomaterials with Biological Systems*, American Scientific Publishers, Los Angeles (2007)
176. N. V. Vallabani, S. Mittal, R. K. Shukla, A. K. Pandey, S. R. Dhakate, R. Pasricha, and A. Dhawan, Toxicity of graphene in normal human lung cells (BEAS-2B), *J. Biomed. Nanotechnol.* 7, 106-107 (2011)
177. K. H. Liao, Y.-S. Lin, C. W. Macosko, and C. L. Haynes, Cytotoxicity of graphene oxide and graphene in human erythrocytes and skin fibroblasts, *ACS Appl. Mater. Interfaces* 3, 2607-2615 (2011)
178. K. Yang, Y. Li, X. Tan, R. Peng, and Z. Liu, Behavior and toxicity of graphene and its functionalized derivatives in biological systems, *Small* 9, 1492-1503 (2013)

179. X. Hu and Q. Zhou, Health and Ecosystem Risks of Graphene, *Chem. Rev.*, 113, 3815–3835 (2013)
180. E. L. K. Chng, and M. Pumera, The toxicity of graphene oxides: dependence on the oxidative methods used, *Chem. Eur. J.*, 19, 8227-8235 (2013).
181. L. Horváth, A. Magrez, M. Burghard, K. Kern, L. Forró, and B. Schwaller, Evaluation of the toxicity of graphene derivatives on cells of the lung luminal surface, *Carbon* 64, 45-60 (2013)